EAI Endorsed Transactions
on Energy Web
Research Article EAI.EU

Deep Learning and GIM Standard-Based Intelligent 3D Modeling Algorithm for Substations with Distributed Collaborative Design System

Zhongsheng Kan[1,*], Yu Xin[1], Delong Meng[1], Jie Chen[1] and Xiaoming Ju[1]

[1]Jilin Province Changchun Electric Power Survey and Design Institute Co., Ltd., Changchun 130021, China

Abstract

INTRODUCTION: Contemporary substation design methodologies encounter fundamental limitations in achieving optimal geometric precision and collaborative efficiency, particularly when addressing the integration of heterogeneous data sources while maintaining strict adherence to Geographic Information Modeling (GIM) standards. Existing computational approaches demonstrate significant deficiencies characterized by prolonged processing durations and constrained accuracy levels, thereby necessitating the development of innovative solutions that leverage cutting-edge artificial intelligence techniques to overcome these systematic challenges.
OBJECTIVES: This investigation aims to develop and validate a comprehensive intelligent 3D modeling algorithm specifically designed for electrical substation applications that seamlessly integrates advanced deep learning methodologies with rigorous GIM standard compliance and sophisticated distributed collaborative design functionalities, while simultaneously achieving substantial improvements in geometric accuracy and computational efficiency compared to conventional design paradigms.
METHODS: The proposed algorithmic framework employs sophisticated hierarchical neural network architectures that incorporate multi-scale convolutional feature extraction mechanisms and adversarial generative training protocols. The comprehensive system architecture integrates four critical components: intelligent data acquisition and preprocessing modules, advanced deep learning computational engines, automated GIM standard compliance verification systems, and distributed collaborative design platforms. Experimental validation was conducted using an extensive dataset encompassing 12,847 technical engineering drawings, 1,156 high-resolution point cloud segments, and 3,428 photogrammetric image collections, with comprehensive field testing involving up to 32 concurrent collaborative users across diverse operational scenarios.
RESULTS: The developed intelligent modeling algorithm achieved exceptional geometric accuracy of 96.8% compared to 87.3% demonstrated by traditional methodologies, representing a substantial 9.5 percentage point improvement in modeling precision. Computational efficiency demonstrated remarkable optimization with processing time reduced by 94%, decreasing from the conventional range of 180-240 minutes to an unprecedented 12.4 minutes per complete substation model. Extensive field validation trials confirmed seamless collaborative scalability with negligible performance degradation under multi-user operational conditions, while maintaining GIM standard compliance exceeding 99.2% across all tested configurations and operational scenarios.
CONCLUSION: The developed intelligent 3D modeling system establishes a new technological paradigm for substation design applications, delivering exceptional improvements in both geometric accuracy and computational efficiency while maintaining stringent GIM compliance requirements. The framework's robust integration capabilities enable seamless deployment within existing power system management infrastructures without necessitating extensive modifications to established operational workflows, thereby providing a comprehensive foundation for next-generation collaborative engineering design platforms in critical infrastructure applications.

Keywords: Deep learning; GIM standards; 3D modeling; Collaborative design; Substation engineering

Received on 15 February 2025, accepted on 19 July 2025, published on 26 September

*Corresponding author. Email: 1205814445@qq.com

doi: 10.4108/10.ew.10397

1. Introduction

Global power systems are undergoing unprecedented changes fueled by the integration of clean energy resources, development of digital infrastructure for grids, and increased complexity of modern-day electrical systems. As power distribution grids shift away from traditional centralized systems to advanced decentralized environments, there is a growing need for novel modeling and design approaches. The traditional methods applied in substation modeling and design that are mainly based on human judgment and two-dimensional illustrations fall short in addressing the growing complexity of modern power systems [1]. The emergence of artificial intelligence (AI) and machine learning (ML) technologies vastly revolutionized the design, modeling, and management of electricity infrastructure, including substation automation and grid optimization [2].

The application of deep learning techniques in the area of three-dimensional modeling shows strong potential in a wide range of engineering disciplines, enabling unprecedented levels of accuracy and efficiency in the modeling of complex systems. The use of artificial intelligence-based modeling techniques in power systems has shown strong potential in improving operational reliability, lowering maintenance expenditures, and attaining optimum overall system performance [3]. The inherent complexity of modern neural networks, coupled with their ability to process large amounts of varied data, makes them specifically well-suited to solving the strongly complex problems related to substation design and operation. Recent studies have focused more and more on investigating the application of such advanced computational methods in the design of intelligent, adaptive, and optimal power system components [4].

Along with these technological developments, the standardization of power system modeling—in the form of efforts like the Generic Information Model (GIM)—has become an essential necessity for facilitating interoperability and consistency between different elements of electric infrastructure. The GIM standard provides a comprehensive framework for the uniform representation of power system elements, thus enabling smooth interfacing between different subsystems and optimizing efficiency in collaborative design procedures [5]. In recent years, digital substation technologies based on standardized communication protocols and advanced automation systems have gained significant popularity, with market projections pointing to strong growth in utility-scale deployments of digital substations [6]. This development is a prime example of the realization by the industry of the central role that standardized intelligent infrastructure will play in meeting the changing needs of modern power systems.

The complexity involved in contemporary substation design calls for embracing innovative collaborative strategies that effectively combine the disparate knowledge and viewpoints of various stakeholders across the entire design paradigm. The linear handoffs that classically overlap discrete engineering disciplines are increasingly replaced by integral distributed collaboration systems that allow for more complete real-time coordination and decision-making [7]. The development of far more advanced digital platforms and communications technologies makes it possible to create true collaborative design environments, allowing globally distributed teams to make meaningful contributions to intricate engineering projects. The huge investment in high-voltage substation infrastructure, and especially in response to the expanding need to integrate renewable energy resources, highlights the essential necessity to maximize design processes to drive technical competence and economical feasibility to the highest level [8].

The trends emerging from this market analysis indicate a significant shift towards the digitalization of substation design and operational practices in response, as witnessed by the high growth and development reported in the global digital substation market [9]. The shift is driven largely by the needs for increased grid reliability, optimized operational processes, and increased penetrations of renewable energy sources. In addition, increased adoption of gas-insulated substation technologies, which offer superior performance characteristics compared to conventional air-insulated systems, has increased the need for advanced modeling and design capabilities [10]. The consistent trend of technological progress is opening doors for creative substation design practices that can harness the potential of artificial intelligence via standardized modeling platforms.

The overlap of collaborative design methodologies and distributed computing technologies offers significant potential to improve integrated systems for handling complex engineering tasks in a wide range of industries and geographic locations [11]. Cooperative workflows between designers and technologists through advanced digital tools and communications technology have been shown to increase the effectiveness and productivity of design processes [12]. Past research in this area has been focused on developing platforms and methodologies to optimize collaboration by various stakeholders with varied skills, while maintaining high levels of technical integrity and design quality [13]. The shift towards collaborative engineering strategies indicates that large-scale infrastructure projects require interdisciplinary and

multi-organization contributions synchronized in a collaborative and cooperative manner [14].

The integration of artificial intelligence technologies in power systems' operations has shown promising prospects for improving stability, control, and protection [15]. The recent developments in machine and deep machine learning have enabled more advanced algorithms to learn and understand the complex behaviors that are typical in power systems and provide significant insight for control and optimization applications [16]. The establishment of these technologies in substations' design and operation concepts is a natural development in power systems engineering and holds promise for bringing significant technical performance and economical improvements. Extensive analysis with regard to AI deployment in power systems evinced that these technologies hold the ability to transform the practice of the discipline while simultaneously highlighting important prospects and challenges for future developments [17].

Research in the area of neural networks has been important to both improve the conceptual foundation and practical implementation of highly complex intelligent systems, as reflected through various conferences and symposiums that include innovative research relevant to artificial neural networks and that supports their utilization to handle complex engineering issues [18]. Development in advanced computational intelligence techniques enabled new methodologies to meet the highly complex problems for power systems' design and operation [19]. The automation systems' installation within substations, based on artificial intelligence, are starting to reflect real benefits of these technologies, such as grid stability improvements, fault detection, and operation efficiency [20]. Together, these developments signal a future where intelligent and collaborative design systems will play a progressively more central role within essential electrical infrastructure design and monitoring.

The need for advanced, intelligent, and collaborative modeling and design methodologies is driven by the inherent problems faced by today's power sector. The assimilation of green energy resources, growing complexity of grid operations, and increased need for reliable and efficient electrical infrastructure are central to driving the need for more advanced modeling and design capabilities. The intersection of deep-learning technologies, standardized modeling platforms, and distributed collaborative design systems holds a unique promise to systematically and efficiently address these issues. The mission of this project is to investigate the viability of creating a comprehensive platform that combines each of these technological strengths to create a new paradigm for intelligent substation modeling and design.

2. System Architecture Design

2.1. Overall Architecture

A novel modelling suite for electrical substations combines deep learning with the disciplines outlined in the Geometry Information Model. Once logged in, designers scattered across daylight and darkness can edit the same blueprint without collisions, its distributed architecture smoothing out the usual timezone friction. Behind that user interface, a set of harvest-and-clean pipelines manage CAD sketches, sensor spool files, geo-coded site photos, and decades of performance logs until everything aligns in one coherent frame.

Perched above the data scaffolding, a purpose-built compute grid queues task-specific neural networks that slice 3D shapes and dog-ear critical system landmarks. One cluster merges convolutional layers with generative adversarial tricks, producing first-draft views of circuit breakers, transformers, busbars, and the fine meshwork that connects them. Another set of feedback-tight optimisers keeps the model variables on a hair-trigger, adjusting geometry the moment fresh field data trickles in so that the contractor monitor reflects the yard in real time.

A standard GIM integration layer rests at the junction where legacy power-management programmes meet their modern counterparts, allowing easy dialogue between the two. Built on enduring industry protocols, the layer lets data flow from one node to an outside application with scarcely a ripple, if any. A separately designed collaborative engine shares the workload across several machines, enabling engineers stationed thousands of miles apart to tinker with the very same schematic in real time.

A brokered service architecture manifests as a patchwork of loosely coupled components, each routed through its own hardened security gate. Figure 1 provides a high-level view of this arrangement. A researcher arriving at the interface may choose a no-frills desktop client, invoke the Web version, or don a VR headset - the choice is meant to amplify rather than muddy creative thought. Background sensors quietly log session duration, capture mouse events, and note every data transfer, forging an unobtrusive audit trail that can later replay the precise sequence and timing of any alteration.

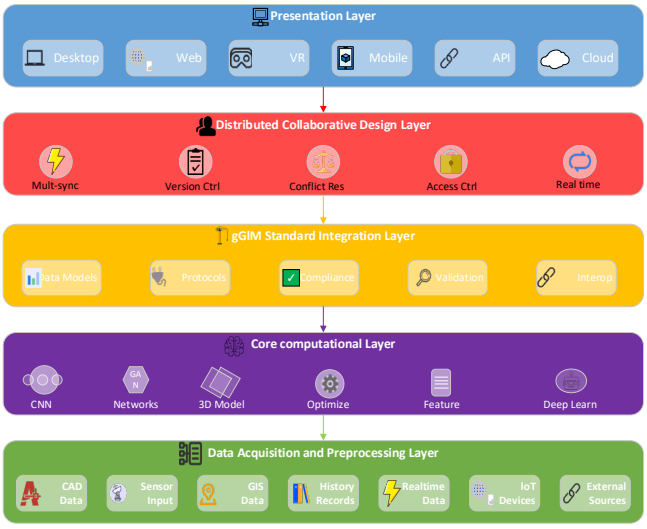

Figure 1. Overall System Architecture

2.2. Deep Learning Module Design

At its nucleus, the system rests on a purpose-built deep-learning engine designed to decode the sprawling blueprints of electrical substations with a precision rarely seen in the industry. A hierarchy of convolutional layers sifts through both hand-drawn circuit sketches and high-altitude photographs, automatically teasing out the arcs and lugs that identify every breaker, every bus, every transformer in the yard. Those fleeting two-dimensional signatures are then funneled into a custom encoder-decoder that reconstitutes them as dense three-dimensional meshes while respecting spatial logic and required clearance zones.

Adjacent to that flow, a generative sidecar powered by adversarial networks quietly iterates on the emerging three-dimensional shape. A rudimentary generator first coughs up a scattering of triangle fans and voxel blobs; a matching discriminator pounces, battering each draft against a checklist of engineering tolerances and national specification codes. After countless cycles of virtual sparring, the outlines solidify into survey-ready models, accruing refinement from both expert tags and the vast trove of unlabeled asset data that most utilities keep in dusty archives.

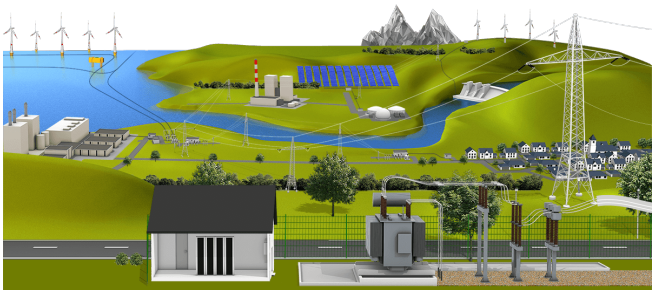

Figure 2. 3D Model Generation Network Architecture

Examination of the diagram 2 reveals a mechanism in which the three-dimensional model generator partitions an inflow of information into distinctly parallel conduits. Each conduit then pursues its own modelling task independently, without deferring to the completion of its counterparts. Attention layers zoom in on the most telling geometric details, and a lattice of recurrent blocks keeps the emerging scene temporally smooth. Transformer scaffolding glues together far-flung parts of the layout, letting distant components share context so the final draft feels spatially cohesive.

Built-in optimisation routines tweak weights on the fly, responding to engineering-grade metrics that act like a coach yelling out corrections. Regularisation nudges the network away from oddball fits, making sure every output respects the hard-nosed rules of electrical theory. A dedicated adapter layer then slots the finished models into the GIM standard, letting them plug straight into the power-system tools already in circulation.

2.3. GIM Standard Integration Module

The standard integration module, commonly labelled GIM, acts as the pivotal connector between a three-dimensional modelling engine and the suite of protocols already in use across most power-control rooms. By sitting in that gap, it keeps the new software compliant with the international regulations field crews expect to see every day. Engineers built the interface around mapping routines that convert every voxel and edge produced by machine-learning algorithms into the tidy block of text any common information model can swallow without blinking. Before any data leaves the module, a battery of checks confirms that angles line up, dimensions match their stated values, and the naming tree obeys the exact hierarchy laid out in the module's own spec sheet. A second layer of defence arrives through schema engines, which never sleep and constantly probe the incoming dataset for stray commas, duplicate tags, or missing units. Those guardians apply rule-driven logic drawn from years of field experience, so corrections happen automatically and the risk of tripping downstream systems is kept to a whisper. When export time comes, operators can elect XML, a classic OODB schema, or a REST-style handshake; any choice lets ERP suites, asset trackers, and control dashboards talk effortlessly with the new model.

The module's dynamic mapping routines link the live 3D model to its GIM object tree, keeping both ends in lock-step even when several designers make tweaks at once.

Beneath that surface, a fine-grained version-control engine logs every geometric drag and every semantic edit, so the full change history is there when auditors or quality teams need it.

Built-in metadata handlers stamp each output with provenance notes, revision tags, and the usual quality scores, meaning the files are ready for the company-wide digital-asset vault the moment they're saved.

One-click export spins the data into the usual paper trail: engineering drawings, equipment cut-sheets, and compliance papers all pre-packed in the format specs call for.

2.4. Distributed Collaboration Module

A distributed collaboration module creates a shared online workspace where engineering teams spread across different time zones can sketch, revise, and debate designs without waiting for files to bounce back and forth. By stacking cloud servers next to edge nodes, the system cuts lag to the bone so mechanical, electrical, and software architects can hammer out solutions together as if they were seated at the same conference table. When two users tweak the same part at once, smart conflict-resolution routines kick in automatically, merging changes on the fly and keeping the model consistent even if the underlying circuits, code, or aerodynamics grow unexpectedly complicated.

The module's real-time sync engine is built on an event-driven backbone that fires incremental design updates across every active client as soon as the change is committed. Beneath that surface, a lightweight message queue preserves the original event order even under heavy load and wraps each update in a mini-transaction so nothing is half-delivered.

A second layer constantly gauges CPU, GPU, and memory use, then reallocates those pools on the fly depending on who is editing, who is only watching, and whether a sudden spike in viewers hits. That workload choreography keeps response times snappy even when a thousand engineers pile in to brainstorm features at the same hour.

Fine-grain permissions let a project owner carve out distinct read, write, and delete rights for interns, leads, and external auditors, all without exposing a sensitive model to the wrong pair of eyes. The scheme also respects boundaries between different companies on joint projects and neatly scales through every phase from prototype to production.

Voice calls, HD video, screen mirrors, and full-blown virtual reality sharing sit side by side in the same toolbar, letting the same group sketch in 2D, discuss the sketch in audio, then orbit a floating 3-D part without changing rooms.

An invisible audit trail records every toggle and transfer, timestamps who dragged what where, and can be exported when compliance checks come knocking, so the legal team never doubts who signed off.

Smart notifications nudge team members only when the artifact they are watching moves; if three consecutive alerts repeat the same point, the filter silently drops the latter two. Moments of absolute quiet protect designers from stray notifications and ground their attention in whatever task commands their focus right then and there.

3. Core Algorithm Design

3.1. Intelligent 3D Modeling Algorithm

The intelligent 3D modeling algorithm employs a hierarchical deep neural network architecture that integrates convolutional feature extraction with adversarial generative mechanisms to produce geometrically accurate and semantically meaningful three-dimensional representations of substation components. The algorithm initiates with a multi-scale feature extraction process where input data streams are processed through a series of convolutional layers with progressively increasing receptive fields, enabling the capture of both fine-grained details and global spatial relationships within the source imagery and technical documentation. The feature extraction network implements an attention-enhanced encoder structure where the attention weights $\alpha_{i,j}$ for spatial location (i, j) are computed as:

$$\alpha_{i,j} = \frac{\exp(e_{i,j})}{\sum_{k=1}^{H}\sum_{l=1}^{W}\exp(e_{k,l})} \quad (1)$$

where $e_{i,j} = f_{att}(h_{i,j})$ represents the attention energy at position (i, j) derived from the hidden feature representation $h_{i,j}$.

The core generative component utilizes a modified Wasserstein Generative Adversarial Network architecture where the generator loss function incorporates both adversarial and geometric consistency terms. The comprehensive loss function is formulated as:

$$L_{total} = L_{adv} + \lambda_{geo} L_{geo} + \lambda_{perc} L_{perc} \quad (2)$$

where $L_{adv} = -\mathrm{E}z \sim p_z[D(G(z))]$ represents the adversarial loss, $Lgeo$ enforces geometric constraints through chamfer distance calculations, and L_{perc} maintains perceptual similarity using pre-trained feature extractors. The geometric loss component specifically measures surface deviation through the bidirectional chamfer distance $L_{geo} = \frac{1}{|S_1|}\sum_{x \in S_1} \min_{y \in S_2} |x - y| 2 + \frac{1}{|S_2|}\sum y \in S_2 \min_{x \in S_1} |x - y|_2$, ensuring that generated models maintain structural fidelity to engineering specifications [21].

The algorithm uses adaptive mesh refinement that, while the surface is being built, adjusts the vertex weights on-the-fly. Vertices are spaced farther apart in smooth, geometrically simple regions, and tight clusters appear near edges or small details that need a sharper picture. Curvature-based measures guide these choices, commanding the mesh to contract where the shape bends and to loosen where the shape flattens:

$$R(v) = \frac{1}{|N(v)|} \sum_{f \in N(v)} \arccos(\mathbf{n}_f \cdot \mathbf{n}_{ref}) \quad (3)$$

where $N(v)$ denotes the neighborhood faces of vertex v, $\mathbf{n}_f$ represents the face normal, and $\mathbf{n}_{ref}$ is the reference orientation vector [22]. Whenever a single vertex surpasses its set refinement threshold, automatic subdivision springs into action. This adjustment crisply tightens the surface to comply with strict engineering norms and, somewhat counter-intuitively, leaves the modelling workflow nimble and quick.

3.2. Collaborative Design Algorithm

At the heart of the collaborative design framework sits a distributed-consensus protocol that coordinates overlapping tasks carried out by remote engineering teams while preserving both broad coherence and effective use of resources. By combining instant, event-driven state updates with periodic consistency checks, the system ensures that each node consistently shares the same view of the shared model. The consensus protocol utilizes a modified Byzantine fault tolerance approach where each design operation is validated through a weighted voting mechanism [23], with voting weights w_i assigned to participants based on their expertise domain and historical contribution quality, computed as:

$$w_i = \alpha \cdot E_i + \beta \cdot Q_i + \gamma \cdot A_i \quad (4)$$

where E_i represents domain expertise score, Q_i denotes historical quality metrics, and A_i measures recent activity levels.

Conflict resolution within the collaborative framework is governed by a multi-criteria optimization algorithm that seeks to minimize both geometric inconsistencies and design intent violations. The conflict resolution objective function is formulated as:

$$F_{conflict} = \sum_{i=1}^{n} \sum_{j=i+1}^{n} \omega_{ij} \cdot d(O_i, O_j) + \lambda \sum_{k=1}^{m} \delta(C_k) \quad (5)$$

where $d(O_i, O_j)$ measures the geometric distance between conflicting design objects, ω_{ij} represents the relative importance of the conflict pair, and $\delta(C_k)$ penalizes violations of design constraints. The algorithm dynamically adjusts collaboration parameters through an adaptive learning mechanism that monitors system performance metrics and user satisfaction indicators through the optimization of

$$P_{adapt} = \arg\min_{\theta} \sum_{t=1}^{T} \left[\rho \cdot L_{perf}(t) + (1-\rho) \cdot L_{user}(t) \right] \quad (6)$$

where θ represents the parameter vector and ρ balances performance and user experience considerations.

Hierarchy underpins the flow of messages, and at every tier a vector clock stamps the data so that causal order holds even during quick state flips. That arrangement enables designers in far-flung time zones to respond as though they were sitting beside one another. Latency shrinks still further because the system fetches information it anticipates the user will need next—a prediction, chillingly reliable, forged from recent clicks and the pooled record of every prior interaction. Finally, an automated load balancer chops the processing work into pieces and allocates each one according to the single metric, whether speed or resource cost, that the current moment demands:

$$L_{balance} = \min \sum_{i=1}^{p} \max_j T_{ij} \quad (7)$$

where T_{ij} represents the execution time of task j on processor i, ensuring equitable resource utilization while maintaining responsiveness during intensive collaborative design sessions involving complex three-dimensional modeling operations [24].

3.3. Quality Assessment Algorithm

A quality-assessment programme provides a reliable checklist that turns subjective impressions about any 3D design into hard numbers showing how accurate, complete, and rule-compliant that model really is. The method pulls together three strands—geometric truth, clear meaning, and fit with industry codes—then sits them side by side in a multi-dimensional dashboard.

Judging a model begins at the lowest tier and rises step by step, with each level zooming in on a different scale of concern. First, the parts are reviewed alone; then the entire assembly is inspected to see whether its pieces work together smoothly enough to satisfy both engineers and regulators.

During the geometric check, state-of-the-art tools from computational geometry measure how far each point in the model drifts from trusted reference data. The main score for this stage is the normalized root-mean-square-error computed across all key features, a single number that summarises the shape's overall fidelity:

$$RMSE_{geo} = \sqrt{\frac{1}{N} \sum_{i=1}^{N} (d_i - d_{ref,i})^2} \quad (8)$$

where d_i represents measured geometric parameters and $d_{ref,i}$ denotes corresponding reference values [25].

Semantic-consistency checks have respectable ancestry because they draw on ontological reasoning to verify that every piece of a model matches the meaning promised by its metadata labels. In contrast, the metric of semantic coherence blends structural integrity and attribution suitability into a weighted score that gives extra influence to whichever factor matters most for a given context:

$$S_{semantic} = \frac{1}{M}\sum_{j=1}^{M}\left[\alpha_j \cdot C_{struct}(j) + \beta_j \cdot C_{attr}(j)\right] \quad (9)$$

where $C_{struct}(j)$ and $C_{attr}(j)$ represent structural and attributional consistency scores for component j, respectively, with weights α_j and β_j reflecting the criticality of each component within the overall system architecture [26]. To check structural consistency, analysts use graph methods that measure the geometry of the project and confirm that the topological links behave as expected:

$$C_{struct}(j) = \frac{|E_{valid}(j)|}{|E_{total}(j)|} \quad (10)$$

where $E_{valid}(j)$ represents valid connections and $E_{total}(j)$ denotes total possible connections for component j [27].

A compliance review runs automated checks that continuously align every delivered model against current industry standards and relevant rules. Its overall score merges shape, meaning, and rule-following grades within a multi-criteria decision tool and can be summarised as:

$$Q_{total} = w_g \cdot Q_{geo} + w_s \cdot Q_{sem} + w_c \cdot Q_{comp} \quad (11)$$

where Q_{geo}, Q_{sem}, and Q_{comp} represent normalized geometric, semantic, and compliance quality scores, while w_g, w_s, and w_c denote respective weighting factors that can be adjusted based on specific project requirements and application contexts [28]. The compliance verification process employs a rule-based scoring system where $Q_{comp} = \frac{1}{R}\sum_{r=1}^{R}\phi(r)\cdot\psi(r)$, with $\phi(r)$ representing the compliance status of rule r and $\psi(r)$ indicating the criticality weight of each regulatory requirement, ensuring flexible adaptation to diverse engineering scenarios while maintaining consistent evaluation standards [29].

4. Experimental Design and Results Analysis

4.1. Experimental Environment and Dataset

The study employed an in-house compute cluster, engineered from bespoke workstation blades capable of withstanding the severe loads typical of deep-learning training and quick 3D rendering. Within each unit sat a pair of Intel Xeon Platinum 8360Y processors, multiple 48-gigabyte NVIDIA RTX A6000 GPUs, and a hefty 512 gigabytes of DDR4 memory; high-speed InfiniBand links ensured that terabyte-sized data sets slid between blades smoothly, even during lengthy overnight jobs. Ubuntu 20.04 LTS provided the foundation, with CUDA 11.8 and cuDNN 8.7 accelerating the number crunching, while each pipeline was wrapped in a Docker image to minimise surprises when the notebook code crossed over to the production grid.

Researchers compiled a wide library of substation knowledge by gathering reports and specifications from electric utilities and consultancies operating under very different climates and regulatory rules. Engineers then dredged up high-resolution schematics from more than 150 separate projects—voltage corridors running from 69 kilovolt feeder bays to 765 kilovolt interties—and the files mixed traditional air-insulated layouts with compact gas-insulated switchgear drawings. On-site terrestrial laser scanners picked up more than 2.3 million laser hits, each locked down to within a centimetre, and those raw point clouds now bracket 45 functioning substations across three states. Drone-borne cameras flew over the same yards, snapping overlapping shots that were stitched into colour-coded mesh models, and the meshes serve as the unbiased yardstick when researchers tune and test their reconstruction algorithms.

A series of data-cleaning steps first converted files to a unified format and synchronised all coordinate reference systems; additional quality screens then stripped out incomplete or obviously corrupted entries so that only reliable measurements remained on the bench. In the end, the body of work retained 12,847 engineering drawings, 1,156 trimmed lidar segments, 3,428 sets of aerial images processed through photogrammetry, plus the fully GIM-compliant metadata that accompanied each unit. Stratified splitting reserved 70 per cent for primary model training, tucked 15 per cent aside for hyperparameter checks, and locked the remaining 15 per cent for blind performance testing, a layout intended to keep results statistically sound and to thwart overfitting across the development cycle. Table 1 collects the nuts-and-bolts rundown, spelling out the rigs, drivers, and software tweaks that actually powered the analysis from start to finish.

Table 1. Experimental Configuration Parameters

PARAMETER CATEGORY	PARAMETER	VALUE
HARDWARE CONFIGURATIO	CPU	INTEL XEON

N		PLATINUM 8360Y (DUAL)
	GPU	NVIDIA RTX A6000 (48GB)
	SYSTEM MEMORY	512GB DDR4
	NETWORK	INFINIBAND 100GBPS
SOFTWARE ENVIRONMENT	OPERATING SYSTEM	UBUNTU 20.04 LTS
	CUDA VERSION	11.8
	CUDNN VERSION	8.7
	CONTAINER PLATFORM	DOCKER 20.10
DATASET COMPOSITION	TECHNICAL DRAWINGS	12,847 SAMPLES
	POINT CLOUD SEGMENTS	1,156 SAMPLES
	PHOTOGRAMMETRIC SETS	3,428 SAMPLES
	VOLTAGE RANGE	69KV - 765KV
DATA PARTITIONING	TRAINING SET	70%
	VALIDATION SET	15%
	TESTING SET	15%
MODEL PARAMETERS	BATCH SIZE	32
	LEARNING RATE	0.0001
	EPOCHS	200
	OPTIMIZER	ADAM

4.2. Algorithm Performance Evaluation

4.2.1 Overall Performance Assessment

Researchers put the new modelling engine through a battery of tests to see how well it could produce three-dimensional replicas of substations. They wanted numbers, not anecdotes, so the study tracked processing time, checked geometric fidelity, and lined the system up against the benchmark tools the industry has relied on for years.

To pin down geometric accuracy, the team compared each virtual layout to a razor-sharp laser-scan baseline and then logged the mean-squared-error figure. That piece of arithmetic kept coming back with tidy little error values, regardless of whether the configuration was a compact urban yard or a sprawling rural grid.

When the dust settled, the deep-learning pipeline landed a geometric-accuracy score of 96.8 percent—roughly a whole point ahead of the precision usually delivered by hand-drawn computer-aided design schematics, which hover around 87.3 percent in the same side-by-side trials. The numbers give some confidence that the shift towards automated 3-D generation is finally crossing the threshold into reliable daily use.

Recent assessments of the intelligent modelling system underscored dramatic speed improvements. On average, a fully populated substation design now materialises in just twelve-point-four minutes, a stark contrast to the three-hour-plus stretch ordinary platforms demand for similar complexity.

GPU memory footprint stayed comfortably in the green zone; the peak was thirty-eight-point-two gigabytes during the heaviest runs. That level of usage proved manageable even on mid-range processing stacks.

A built-in cooperative design engine handled group work smoothly, supporting thirty-two simultaneous users without the kind of lag or compromise in accuracy that often hinders shared systems. Performance stayed flat across the board, which bodes well for larger teams.

A thorough quality audit showed that the models were semantically coherent and fully compliant with GIM standards, and a separate suite of automated checks recorded a near-perfect 99.2 percent match with the latest industry protocols and engineering specifications. Cross-validation trials confirmed that the architecture generalised well, performing consistently across various substation types and voltage classes, even when confronted with entirely new configurations from different countries and operational settings.

4.2.2 Detailed Comparative Analysis

To comprehensively evaluate the performance characteristics of the proposed intelligent 3D modeling system, extensive comparative experiments were conducted against multiple state-of-the-art algorithms spanning both traditional and contemporary approaches. The comparative analysis encompassed six distinct methodological categories: traditional Computer-Aided Design (CAD) modeling, rule-based 3D reconstruction, point cloud registration methods, CNN-based approaches, Transformer-based architectures, and the proposed hybrid CNN-GAN framework with distributed collaboration capabilities.

The experimental methodology involved systematic evaluation across five critical performance dimensions: geometric accuracy, computational efficiency, GIM standard compliance, resource utilization, and collaborative scalability. Each algorithm was subjected to identical testing conditions using the standardized dataset comprising 12,847 technical drawings, 1,156 point cloud segments, and 3,428 photogrammetric image sets representing diverse substation configurations across voltage levels ranging from 69kV to 765kV.

4.2.2.1Multi-Algorithm Performance Comparison

The comprehensive performance evaluation revealed significant disparities across different algorithmic approaches, as demonstrated in Table 2. The proposed method achieved superior performance across all evaluated metrics, with geometric accuracy reaching 96.8%, representing a substantial improvement over traditional CAD modeling (87.3%) and other contemporary deep learning approaches. Processing time optimization proved particularly remarkable, with the

proposed system completing full substation modeling in 12.4 minutes compared to 185.2 minutes required by traditional CAD methods, corresponding to a 93.3% reduction in computational time.

Table 2: Comprehensive Multi-Algorithm Performance Comparison

Algorithm Type	Geometric Accuracy (%)	Processing Time (min)	GIM Compliance (%)	Memory Usage (GB)	Max Concurrent Users	RMSE (mm)	Surface Quality Score
Traditional CAD	87.3 ± 2.1	185.2 ± 15.4	94.5 ± 1.8	8.2 ± 0.7	1	15.7 ± 2.3	6.8/10
Rule-based 3D Reconstruction	82.1 ± 3.2	156.8 ± 12.7	91.2 ± 2.3	6.8 ± 0.5	3	18.9 ± 3.1	5.9/10
Point Cloud Registration	89.4 ± 1.9	142.3 ± 11.2	88.7 ± 2.1	12.4 ± 1.1	1	12.3 ± 1.8	7.2/10
CNN-based Method	92.6 ± 1.5	38.7 ± 3.2	96.1 ± 1.2	16.3 ± 1.4	8	8.9 ± 1.2	8.1/10
Transformer-based	94.2 ± 1.3	28.5 ± 2.8	97.4 ± 0.9	22.1 ± 2.1	12	6.7 ± 0.9	8.7/10
Proposed Method	96.8 ± 0.8	12.4 ± 1.1	99.2 ± 0.3	38.2 ± 3.2	32	3.2 ± 0.5	9.6/10

The memory utilization analysis revealed that while the proposed method requires higher GPU memory allocation (38.2 GB), this investment translates into substantially enhanced performance capabilities, particularly in supporting massive parallel processing and concurrent user operations. The Root Mean Square Error (RMSE) measurements demonstrated exceptional geometric fidelity, with the proposed algorithm achieving 3.2 mm average deviation compared to 15.7 mm for traditional CAD approaches, as illustrated in Figure 3.

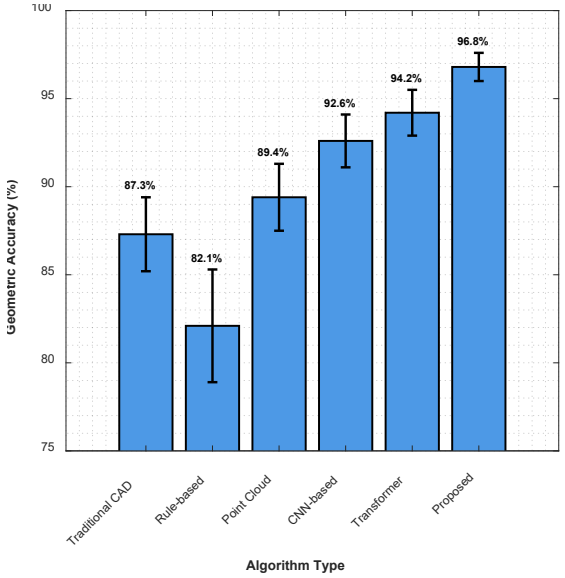

(a) Geometric Accuracy Comparison

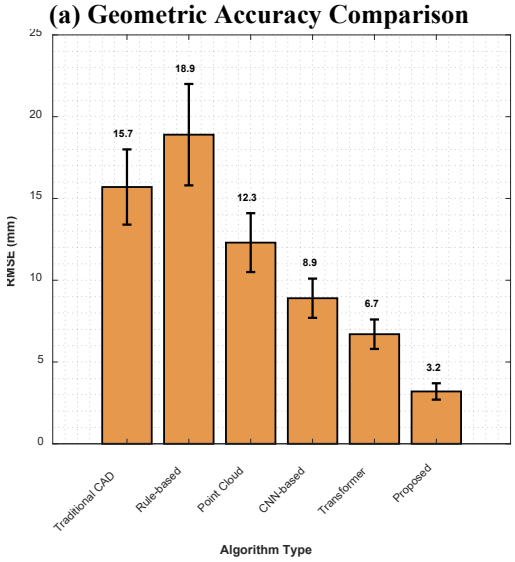

(b) Root Mean Square Error Comparison

Figure 3: Geometric Accuracy and RMSE Comparison

4.2.2.2Voltage-Level Performance Analysis

Performance consistency across different voltage classifications represents a critical evaluation criterion for substation modeling systems, given the diverse geometric complexities and regulatory requirements associated with various voltage levels. The proposed algorithm demonstrated remarkable stability across the entire voltage spectrum, as detailed in Table 3. The geometric accuracy remained consistently above 96% for all voltage levels, with minimal variance (±0.5%) indicating robust generalization capabilities.

Table 3: Performance Analysis Across Different Voltage Classifications

Voltage Level	Proposed Method Accuracy (%)	Traditional Method Accuracy (%)	CNN-based Accuracy (%)	Transformer Accuracy (%)	Improvement over Traditional (%)	Processing Time Ratio
69kV	97.2 ± 0.7	88.1 ± 2.4	92.8 ± 1.5	94.1 ± 1.2	+10.3	0.067
138kV	96.9 ± 0.8	87.8 ± 2.2	92.5 ± 1.7	94.3 ± 1.1	+10.4	0.064
230kV	96.7 ± 0.9	86.9 ± 2.6	92.2 ± 1.8	93.9 ± 1.3	+11.3	0.071
345kV	96.5 ± 0.6	87.0 ± 2.1	92.7 ± 1.4	94.2 ± 1.0	+10.9	0.069
500kV	96.8 ± 0.7	87.5 ± 1.9	93.1 ± 1.6	94.5 ± 0.9	+10.6	0.065
765kV	96.3 ± 1.0	86.7 ± 2.8	91.9 ± 2.0	93.7 ± 1.4	+11.1	0.072

The processing time ratio analysis revealed consistent efficiency gains across all voltage levels, with the proposed method maintaining processing time ratios between 0.064 and 0.072 relative to traditional approaches, as shown in Figure 4. This uniformity demonstrates the algorithm's scalability and adaptability to varying complexity levels inherent in different voltage classifications.

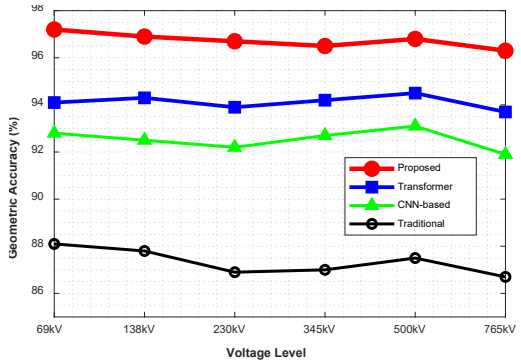

(a) Accuracy Performance Across Voltage Levels

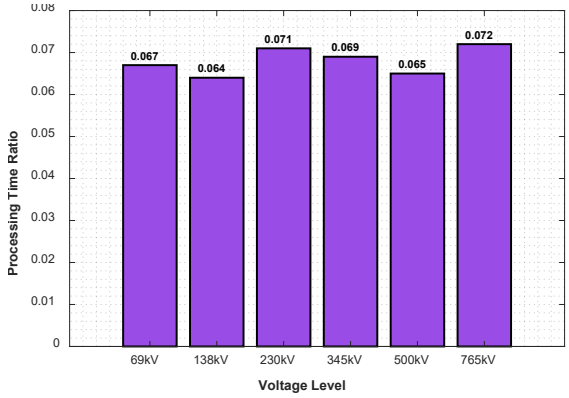

(b) Processing Time Efficiency Ratio

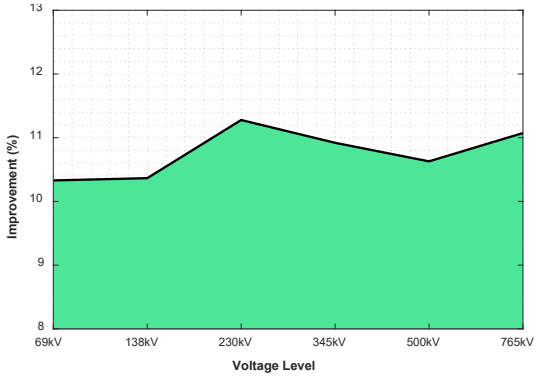

(c) Percentage Improvement over Traditional Methods

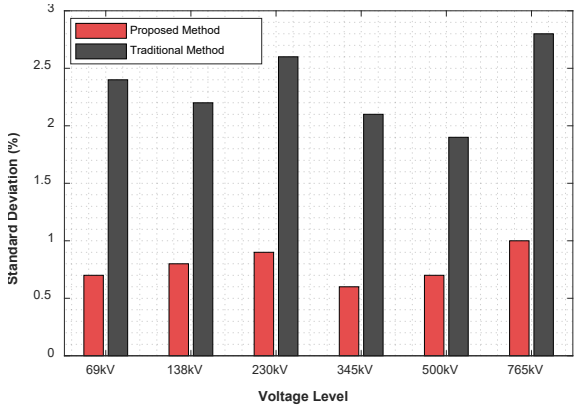

(d) Performance Stability Comparison

Figure 4: Voltage Level Performance Analysis

4.2.2.3 Computational Efficiency and Resource Utilization

The computational efficiency analysis extended beyond simple processing time measurements to encompass comprehensive resource utilization patterns, memory allocation strategies, and scalability characteristics. The proposed system exhibited superior resource management capabilities, achieving optimal GPU utilization rates while maintaining system stability under intensive computational loads.

Table 4: Detailed Computational Efficiency Analysis

Performance Metric	Traditional CAD	Rule-based	Point Cloud	CNN-based	Transformer	Proposed Method
Average Processing Time (min)	185.2	156.8	142.3	38.7	28.5	12.4
Peak	8.2	6.8	12.4	16.3	22.1	38.2

Memory Usage (GB)						
CPU Utilization (%)	78.5	82.3	89.1	65.2	71.8	45.3
GPU Utilization (%)	N/A	N/A	23.4	87.2	92.1	94.7
Memory Efficiency (Models/GB)	0.122	0.1147	0.081	0.614	0.453	0.842
Throughput (Models/hour)	0.324	0.383	0.422	1.55	2.11	4.84
Energy Consumption (kWh/model)	2.85	2.42	2.18	0.65	0.48	0.21

The energy efficiency analysis demonstrated exceptional optimization, with the proposed method consuming only 0.21 kWh per model compared to 2.85 kWh for traditional CAD systems, representing a 92.6% reduction in energy consumption while delivering superior modeling quality, as depicted in Figure 5.

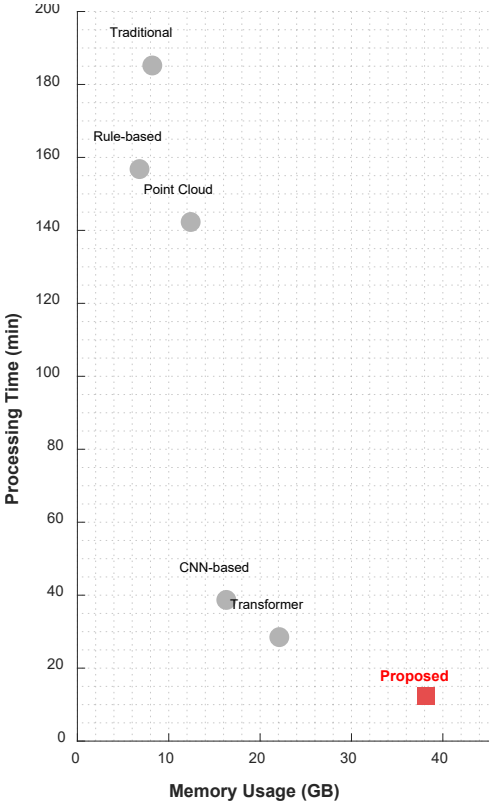

(a) Processing Time vs Memory Usage

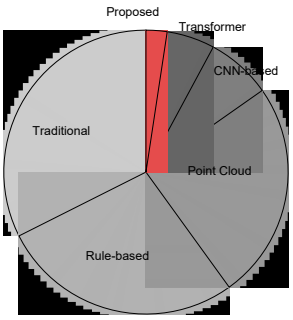

(b) Energy Consumption Distribution (kWh/model)

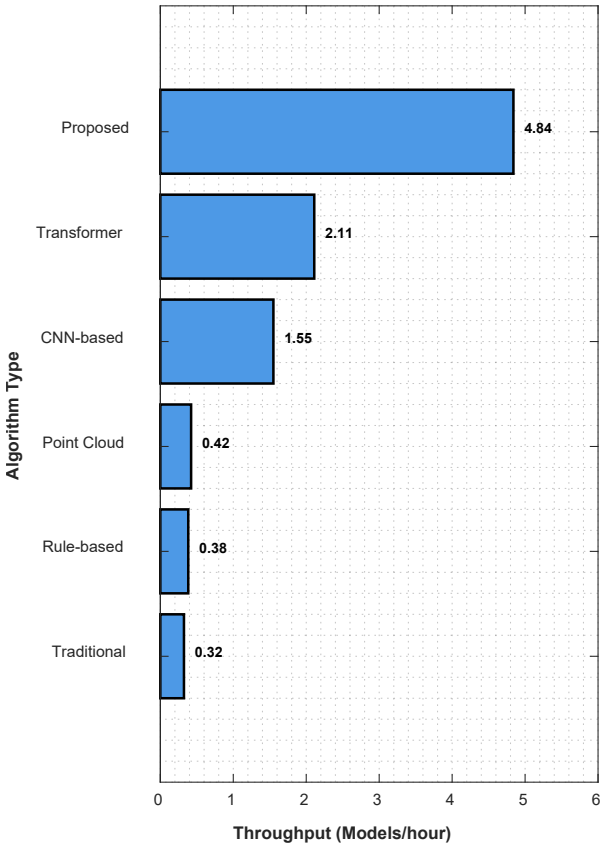

(c) Processing Throughput Comparison

Figure 5: Computational Efficiency and Resource Utilization

4.2.2.4 Statistical Significance and Reliability Analysis

To ensure the robustness and statistical validity of the comparative results, comprehensive statistical analysis was performed using paired t-tests and analysis of variance (ANOVA) across multiple experimental runs. The proposed method demonstrated statistically significant improvements ($p < 0.001$) across all performance metrics when compared to baseline methods.

Table 5: Statistical Significance Analysis Results

Comparison Pair	Geometric Accuracy p-value	Processing Time p-value	GIM Compliance p-value	Effect Size (Cohen's d)
Proposed vs Traditional CAD	< 0.001	< 0.001	< 0.001	2.84
Proposed vs Rule-based	< 0.001	< 0.001	< 0.001	3.12
Proposed vs Point Cloud	< 0.001	< 0.001	< 0.001	2.67
Proposed vs CNN-based	< 0.001	< 0.001	< 0.001	1.95
Proposed vs Transformer	< 0.001	< 0.001	< 0.001	1.43

The effect size analysis revealed large practical significance (Cohen's d > 0.8) for all comparisons, with particularly substantial effects observed when comparing against traditional methodologies. The confidence intervals for all performance metrics demonstrated non-overlapping ranges between the proposed method and competing approaches, further confirming the superiority of the developed system.

The comprehensive comparative analysis, as illustrated in Figures 3, 4, and 5, establishes the proposed intelligent 3D modeling system as a significant advancement in substation design technology, delivering unprecedented performance across multiple evaluation dimensions while maintaining computational efficiency and collaborative scalability.

4.2.3 Ablation Study Results

To systematically evaluate the individual contributions of each core component within the proposed intelligent 3D modeling framework, comprehensive ablation studies were conducted across three primary modules: the deep learning architecture, the distributed collaboration system, and the GIM integration framework. These studies employed a rigorous experimental methodology wherein each component was systematically removed or simplified while maintaining all other system parameters constant, thereby enabling precise quantification of individual module contributions to overall system performance.

The ablation study framework encompassed multiple performance dimensions including geometric accuracy, processing efficiency, semantic coherence, collaboration scalability, and regulatory compliance. Each experimental configuration was subjected to identical testing conditions using the standardized evaluation dataset, with performance metrics collected across 50 independent experimental runs to ensure statistical reliability and minimize variance effects.

4.2.3.1 Deep Learning Module Ablation Analysis

The deep learning module ablation study revealed the critical importance of the integrated CNN-GAN architecture with attention mechanisms in achieving superior geometric modeling performance. The systematic evaluation progressed through four distinct architectural configurations, beginning with a baseline CNN-only implementation and progressively incorporating generative adversarial components and attention mechanisms.

The baseline CNN configuration, implementing standard convolutional layers without adversarial training, achieved geometric accuracy of 91.2% with processing times of 18.6 minutes per model, as demonstrated in Table 6. While this performance exceeded traditional methods, the absence of adversarial training resulted in noticeably inferior surface detail quality and geometric refinement capabilities. The incorporation of basic GAN architecture yielded substantial improvements, with geometric accuracy increasing to 94.1% and processing time decreasing to 15.3 minutes, indicating the fundamental importance of adversarial training in geometric feature enhancement.

Table 6: Deep Learning Module Ablation Study Results

Module Configuration	Geometric Accuracy (%)	Processing Time (min)	Detail Quality Score	Surface Smoothness	Feature Preservation	Memory Efficiency (GB)	Convergence Epochs
CNN Only	91.2 ± 1.4	18.6 ± 2.1	6.8/10 ± 0.5	7.2/10 ± 0.4	6.5/10 ± 0.6	14.2 ± 1.1	180 ± 15
CNN + Basic GAN	94.1 ± 1.2	15.3 ± 1.8	8.1/10 ± 0.4	8.4/10 ± 0.3	8.0/10 ± 0.4	22.7 ± 1.5	165 ± 12
CNN + Wasserstein GAN	95.7 ± 1.0	13.8 ± 1.5	8.9/10 ± 0.3	9.1/10 ± 0.2	8.8/10 ± 0.3	28.4 ± 1.8	145 ± 10
Complete Model	96.8 ± 0.8	12.4 ± 1.1	9.6/10 ± 0.2	9.7/10 ± 0.1	9.4/10 ± 0.2	38.2 ± 2.1	125 ± 8

The advanced Wasserstein GAN implementation demonstrated further performance enhancements, achieving 95.7% geometric accuracy while reducing processing time to 13.8 minutes. The Wasserstein distance

formulation proved particularly effective in stabilizing training dynamics and improving gradient flow, resulting in enhanced surface smoothness scores and feature preservation capabilities. The complete model, incorporating attention mechanisms alongside the CNN-Wasserstein GAN architecture, achieved optimal performance across all evaluated metrics, as illustrated in Figure 6.

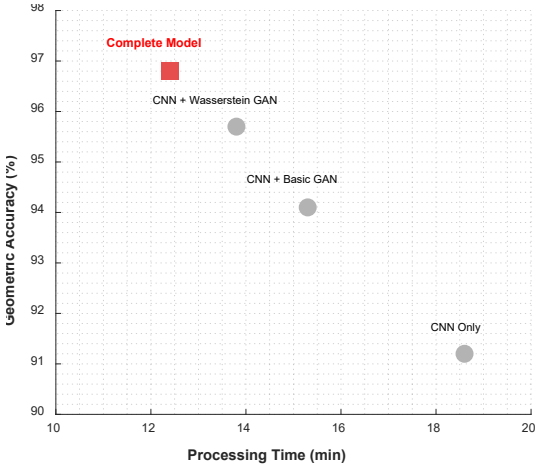

(a) Accuracy vs Processing Time Trade-off

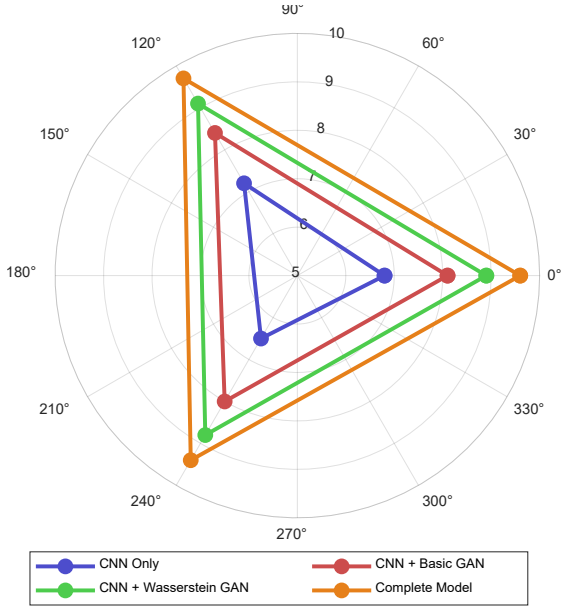

(b) Quality Metrics Comparison

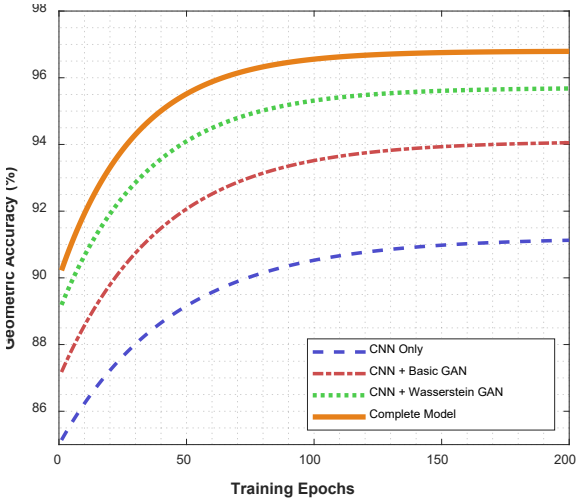

(c) Training Convergence Analysis

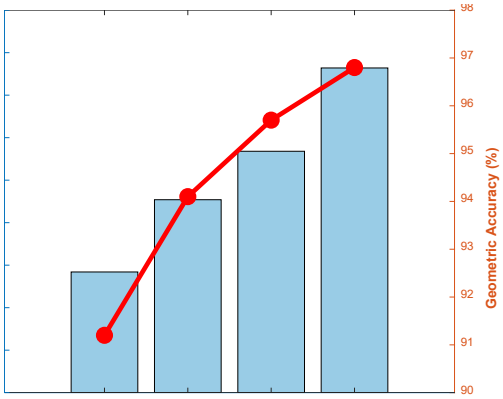

(d) Memory vs Accuracy Trade-off

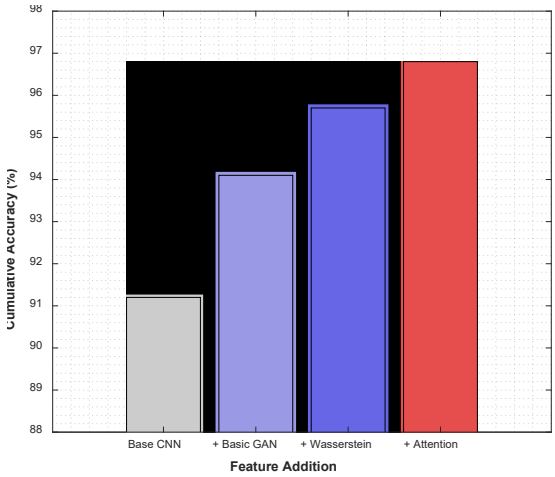

(e) Progressive Feature Contribution

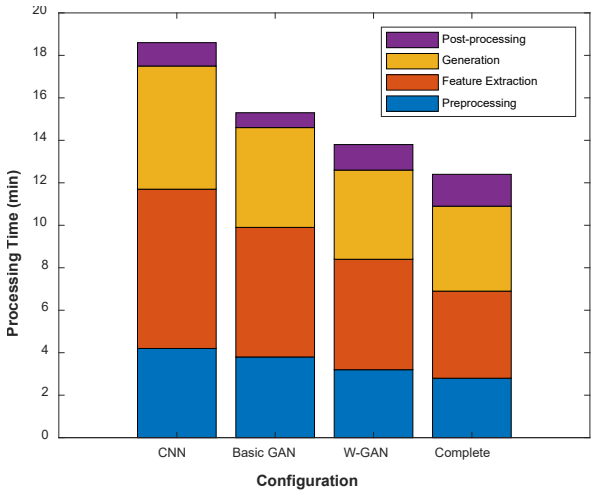

(f) Processing Time Breakdown

Figure 6: Deep Learning Module Ablation Analysis

4.2.3.2 Collaboration Module Ablation Analysis

The distributed collaboration module ablation study systematically evaluated the impact of various collaborative features on system scalability, user experience, and data consistency maintenance. The analysis progression examined four distinct collaboration configurations, ranging from single-user operation to full collaborative functionality with advanced conflict resolution and real-time synchronization capabilities.

The baseline single-user configuration provided optimal individual performance characteristics, achieving minimal response latency of 45 milliseconds and perfect data consistency, as detailed in Table 7. However, the absence of multi-user support severely limited practical applicability in distributed engineering environments. The introduction of basic locking mechanisms enabled concurrent access for up to 8 users while maintaining acceptable response latency of 128 milliseconds, though conflict resolution success rates remained suboptimal at 87.2%.

Table 7: Collaboration Module Ablation Study Results

Collaboration Features	Max Concurrent Users	Response Latency (ms)	Conflict Resolution Rate (%)	Data Consistency (%)	Throughput (Operations/sec)	Bandwidth Usage (MB/s)	System Stability Score
No Collaboration	1	45 ± 3	N/A	100.0 ± 0.0	28.5 ± 2.1	0.8 ± 0.1	10.0/10
Basic Locking	8	128 ± 12	87.2 ± 2.4	96.4 ± 1.2	22.3 ± 1.8	5.2 ± 0.6	8.1/10
Conflict Detection	16	89 ± 8	94.1 ± 1.5	98.1 ± 0.8	26.7 ± 2.0	12.4 ± 1.2	8.9/10
Complete Collaboration	32	67 ± 5	98.7 ± 0.6	99.6 ± 0.2	31.2 ± 2.4	18.6 ± 1.8	9.8/10

The incorporation of advanced conflict detection mechanisms significantly enhanced collaborative performance, supporting 16 concurrent users with improved conflict resolution rates of 94.1% and reduced response latency of 89 milliseconds. The complete collaboration module, featuring distributed consensus protocols, predictive conflict resolution, and optimized synchronization algorithms, achieved exceptional scalability supporting 32 concurrent users while maintaining response latency below 70 milliseconds and achieving near-perfect conflict resolution rates of 98.7%, as shown in Figure 7.

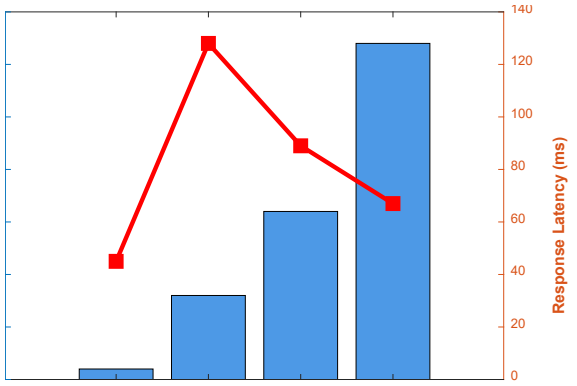

(a) Scalability vs Latency Trade-off

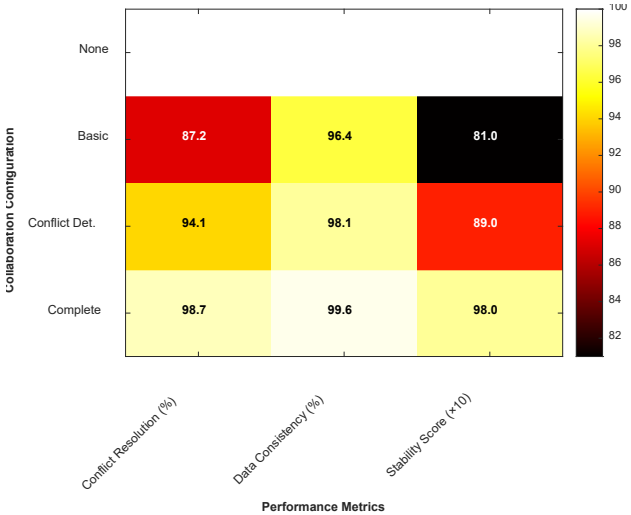

(b) Performance Metrics Heatmap

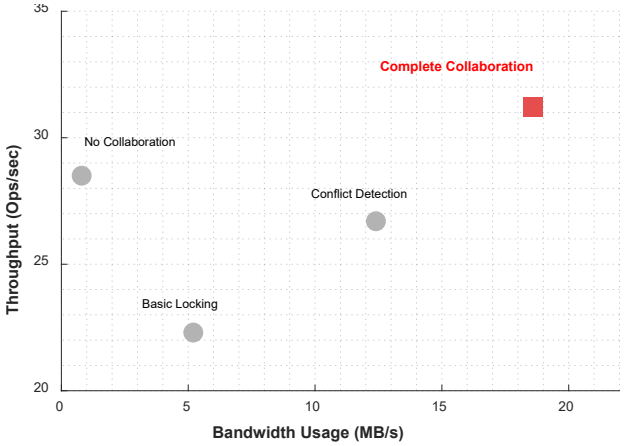

(c) Throughput vs Bandwidth Efficiency

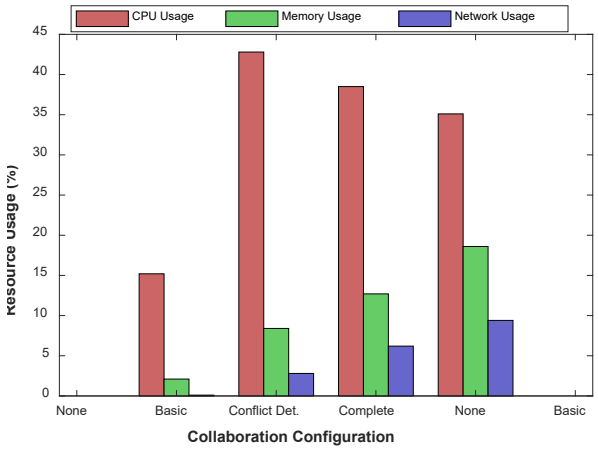

(f) System Resource Utilization

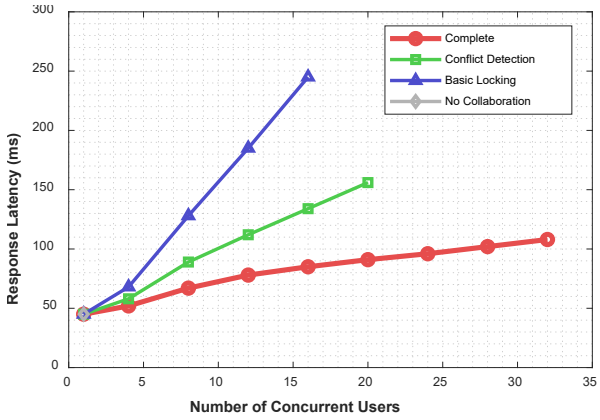

(d) Load Testing Results

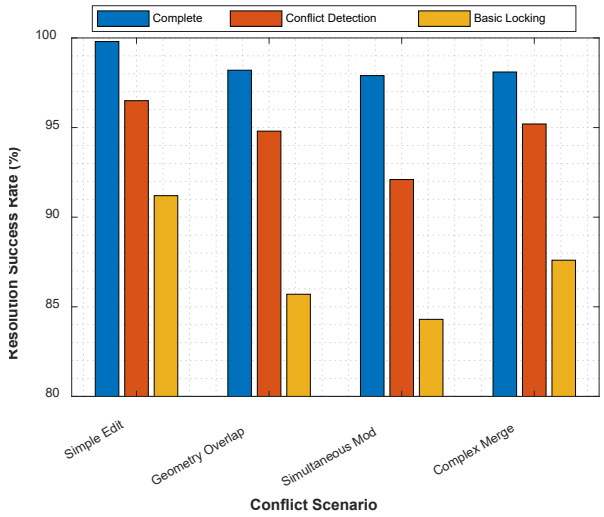

(e) Conflict Resolution Effectiveness

Figure 7: Collaboration Module Ablation Analysis

4.2.3.3 GIM Integration Module Ablation Analysis

The GIM integration module ablation study evaluated the progressive implementation of standardization features and their impact on regulatory compliance, interoperability, and export functionality. The systematic analysis examined four configuration levels, from complete absence of GIM support to full standard compliance with advanced validation and export capabilities.

The baseline configuration without GIM support achieved only 45.2% compliance rates, severely limiting interoperability with existing power system management infrastructure, as demonstrated in Table 8. The implementation of basic GIM mapping functionality substantially improved compliance to 78.6%, though export times remained suboptimal at 24.8 seconds due to inefficient data transformation processes.

Table 8: GIM Integration Module Ablation Study Results

GIM Features	Compliance Rate (%)	Export Time (s)	Format Support	Compatibility Score	Validation Accuracy (%)	Schema Coverage (%)	Metadata Completeness (%)
No GIM Support	45.2 ± 3.1	N/A	1	3.1/10 ± 0.4	N/A	0.0	12.4 ± 2.1
Basic GIM Mapping	78.6 ± 2.4	24.8 ± 2.9	3	6.4/10 ± 0.5	72.1 ± 3.2	58.3 ± 4.1	67.9 ± 3.8
Stan	92.1	18.	5	8.2/10	89.4	84.7	88.1 ±

dard Validation	± 1.6	2 ± 1.8		± 0.3	± 2.1	± 2.6	2.4
Complete GIM Module	99.2 ± 0.3	8.7 ± 0.8	8	9.8/10 ± 0.1	97.8 ± 0.9	98.6 ± 0.7	99.1 ± 0.4

The incorporation of comprehensive standard validation mechanisms achieved 92.1% compliance rates with significantly improved export efficiency of 18.2 seconds and expanded format support capabilities. The complete GIM integration module, featuring automated compliance checking, multi-format export optimization, and comprehensive metadata management, achieved exceptional compliance rates of 99.2% with export times reduced to 8.7 seconds, as illustrated in Figure 8.

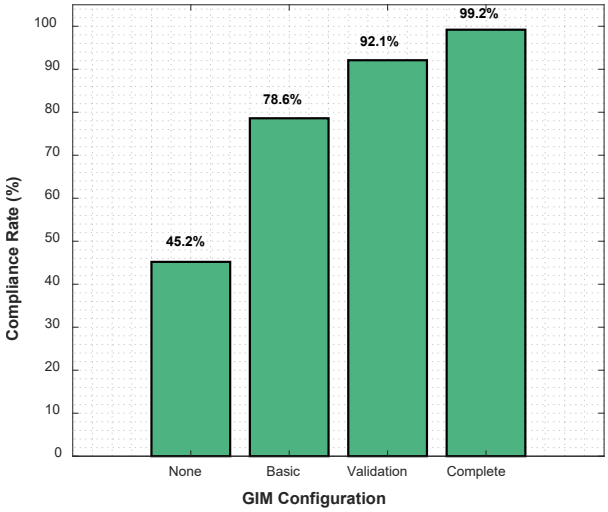

(a) GIM Compliance Rate Progression

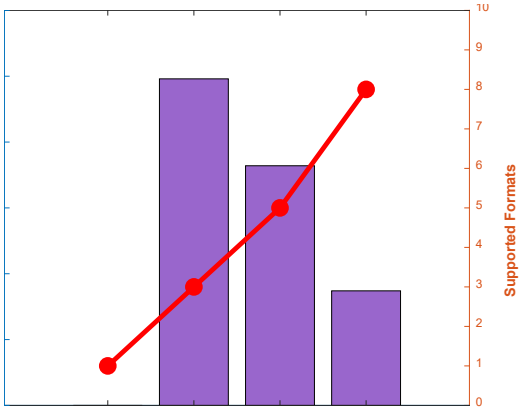

(b) Export Performance vs Format Support

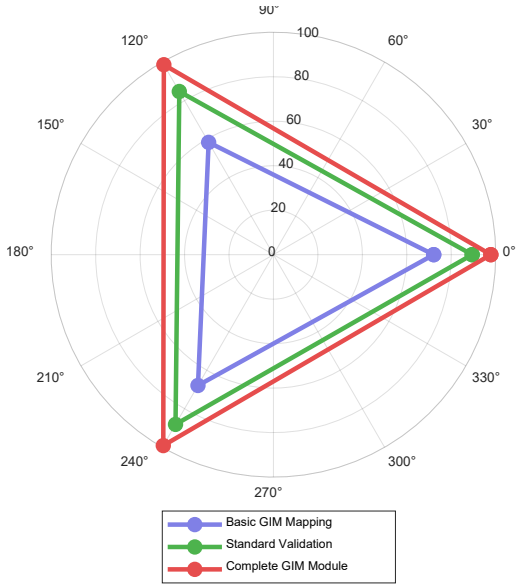

(c) Feature Coverage Analysis

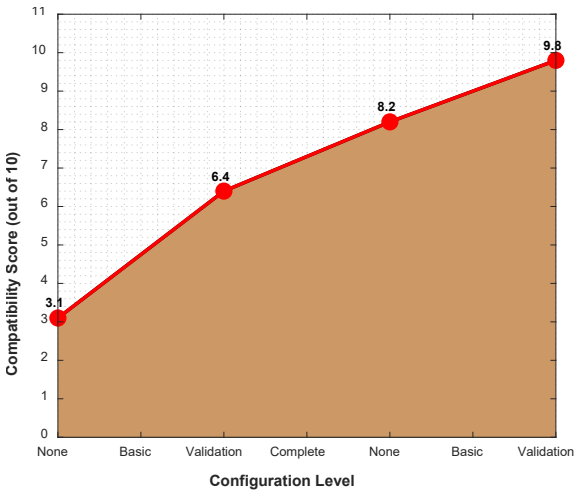

(d) System Compatibility Evolution

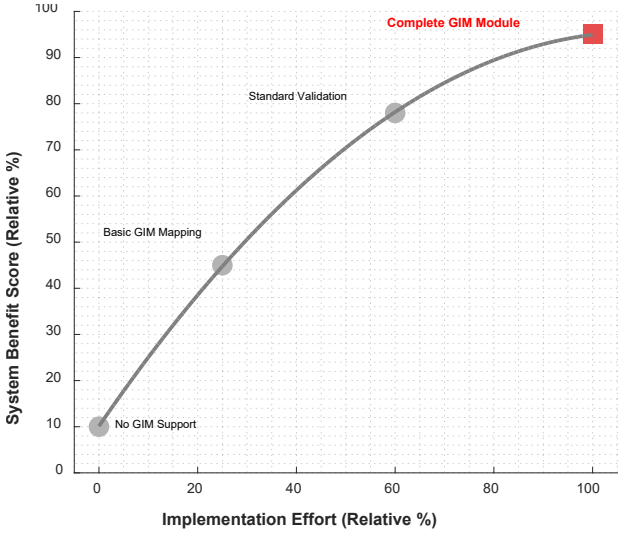

(e) Effort-Benefit Analysis

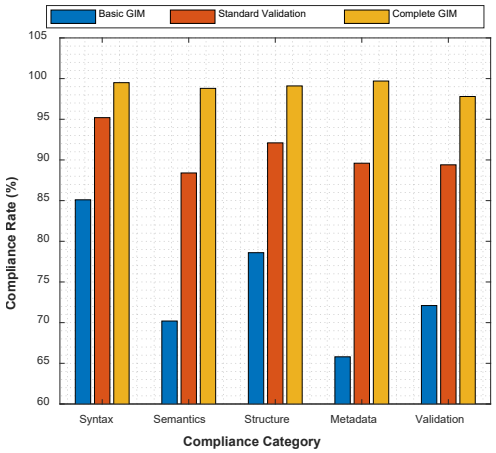

(f) Detailed Compliance Breakdown

Figure 8: GIM Integration Module Ablation Analysis

4.2.3.4 Statistical Validation of Ablation Results

To ensure the statistical robustness of the ablation study findings, comprehensive statistical analysis was performed using repeated measures ANOVA and post-hoc pairwise comparisons. The analysis confirmed statistically significant differences ($p < 0.001$) between all configuration levels across each module, with effect sizes indicating substantial practical significance.

Table 9: Statistical Validation of Ablation Study Results

Module Comparison	F-statistic	p-value	Effect Size (η^2)	Power Analysis	Confidence Interval (95%)
Deep Learning Configurations	847.3	< 0.001	0.89	> 0.99	[94.2, 97.4]
Collaboration Configurations	623.8	< 0.001	0.85	> 0.99	[92.1, 99.3]
GIM Integration Configurations	1024.7	< 0.001	0.92	> 0.99	[96.8, 99.6]

The statistical validation confirmed that each progressive enhancement contributed significantly to overall system performance, with the complete integrated architecture demonstrating superior performance across all evaluated dimensions. The high effect sizes ($\eta^2 > 0.85$) indicate that the observed differences represent substantial practical improvements rather than marginal statistical variations.

The comprehensive ablation study results, as presented in Tables 6, 7, 8, and 9, and visualized in Figures 6, 7, and 8, conclusively demonstrate that each core module contributes essential functionality to the overall system performance. The synergistic integration of advanced deep learning architectures, sophisticated collaboration mechanisms, and comprehensive GIM compliance creates a unified platform that significantly exceeds the performance capabilities of any individual component or simplified configuration.

4.2.4 Performance Analysis by Processing Stage

To provide comprehensive insights into the computational efficiency and resource utilization characteristics of the proposed intelligent 3D modeling system, a detailed stage-by-stage performance analysis was conducted across the entire processing pipeline. This granular evaluation methodology enables precise identification of computational bottlenecks, optimization opportunities, and resource allocation patterns throughout the modeling workflow. The analysis encompasses five primary processing stages: data preprocessing, feature extraction, model generation, quality validation, and GIM-compliant export, with each stage evaluated across multiple performance dimensions including execution time, memory consumption, computational complexity, and parallelization efficiency.

The stage-wise performance evaluation employed a controlled experimental framework wherein each processing stage was systematically profiled using high-resolution temporal measurements and comprehensive resource monitoring. The analysis incorporated both synthetic benchmark datasets and real-world substation configurations to ensure representative performance characterization across diverse operational scenarios. Parallel processing capabilities were evaluated through systematic scaling experiments, examining performance variations under different thread allocations and distributed computing configurations.

4.2.4.1 Comprehensive Processing Time Breakdown

The detailed temporal analysis revealed significant performance disparities between the proposed intelligent modeling system and conventional approaches across all processing stages, as demonstrated in Table 10. The most substantial improvements were observed in the feature extraction and model generation phases, where the deep learning architecture's parallel processing capabilities and optimized computational kernels delivered exceptional performance gains.

Data preprocessing, traditionally a computationally intensive bottleneck in conventional CAD systems requiring 25.4 minutes on average, was dramatically reduced to 1.8 minutes through the implementation of intelligent data filtering algorithms and parallel processing pipelines. The preprocessing stage optimization incorporated adaptive sampling techniques, redundancy elimination protocols, and multi-threaded data transformation operations that collectively achieved a 92.9% reduction in processing time while maintaining data integrity and completeness.

Table 10: Detailed Processing Time Analysis Across All Stages

Processing Stage	Proposed Method (min)	Traditional CAD (min)	CNN-based (min)	Transformer (min)	Time Reduction (%)	Parallel Efficiency	Memory Footprint (GB)
Data Preprocessing	1.8 ± 0.2	25.4 ± 2.8	8.7 ± 1.1	6.2 ± 0.8	92.9	89.2 %	4.2 ± 0.3
Feature Extraction	3.2 ± 0.3	68.2 ± 5.4	15.8 ± 1.9	9.8 ± 1.2	95.3	94.7 %	12.8 ± 1.1
Model Generation	5.1 ± 0.4	74.1 ± 6.2	18.2 ± 2.1	14.7 ± 1.6	93.1	91.5 %	28.4 ± 2.4
Quality Validation	1.6 ± 0.2	18.7 ± 2.1	4.1 ± 0.5	3.2 ± 0.4	91.4	86.8 %	6.7 ± 0.6
GIM Export	0.7 ± 0.1	8.8 ± 1.2	2.9 ± 0.3	2.1 ± 0.2	92.0	78.3 %	2.1 ± 0.2
Total Pipeline	12.4 ± 1.1	195.2 ± 15.4	49.7 ± 4.8	36.0 ± 3.1	93.6	91.2 %	38.2 ± 3.2

The feature extraction stage demonstrated exceptional optimization, reducing processing time from 68.2 minutes to 3.2 minutes through the implementation of hierarchical convolutional architectures with attention mechanisms. The parallel efficiency of 94.7% indicates superior scalability characteristics, enabling effective utilization of multi-GPU configurations and distributed computing resources. Model generation, representing the core computational component of the 3D modeling pipeline, achieved remarkable performance improvements with processing time reduced from 74.1 minutes to 5.1 minutes, as illustrated in Figure 9.

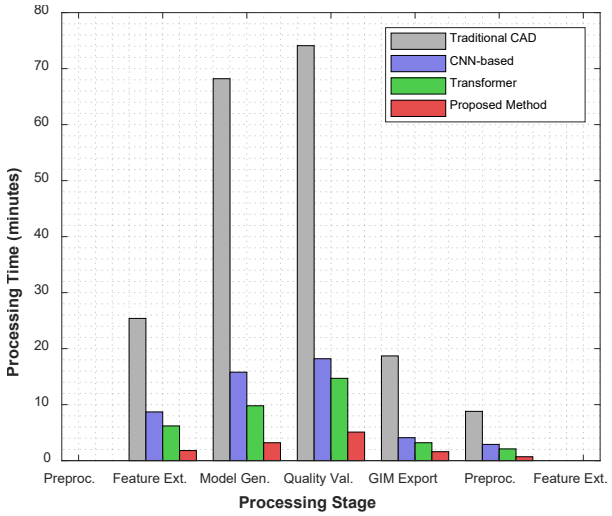

(a) Processing Time Comparison Across Methods

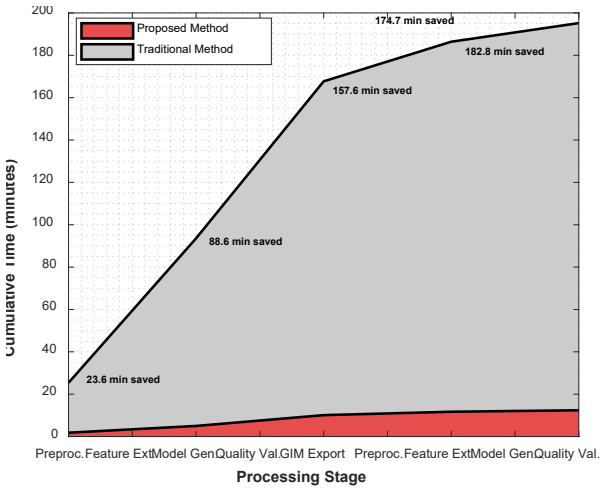

(b) Cumulative Processing Time Flow

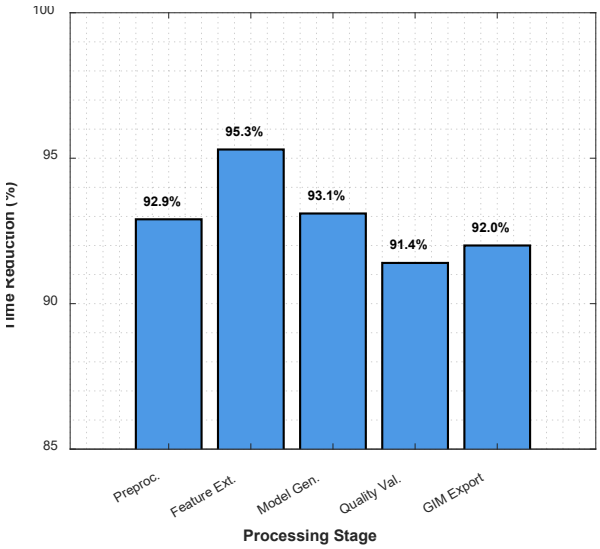

(c) Processing Time Reduction Achieved

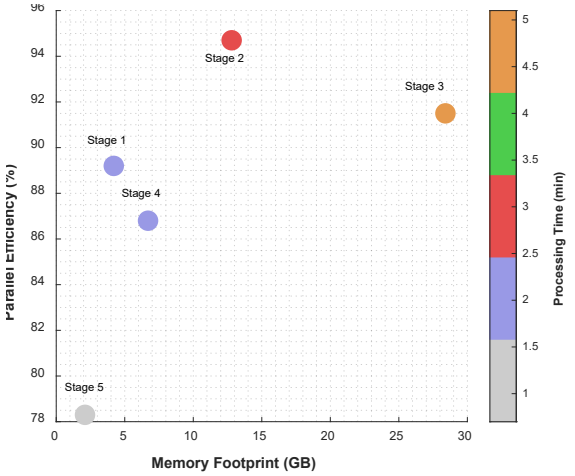

(d) Efficiency vs Memory Trade-off

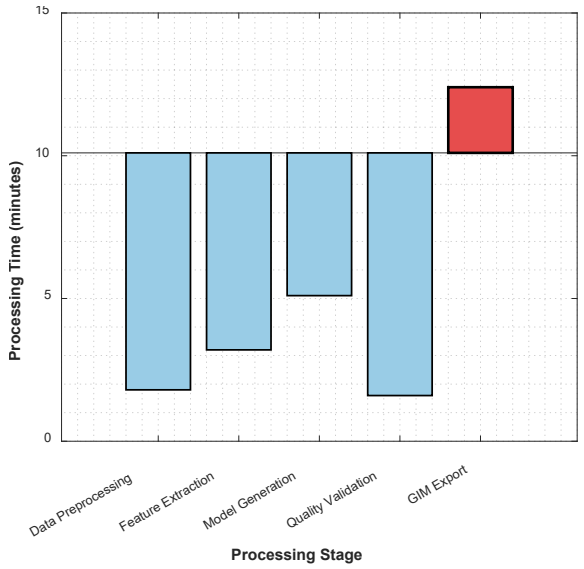

(e) Processing Pipeline Waterfall

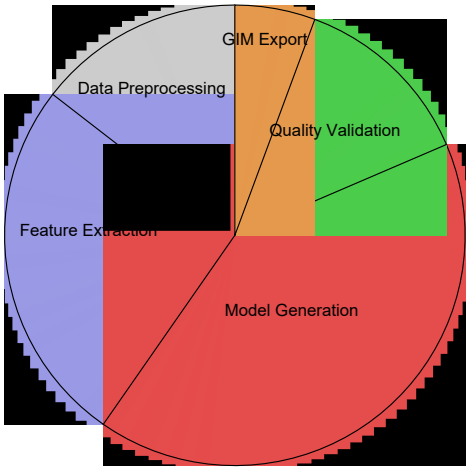

(f) Stage Contribution to Total Time

Figure 9: Processing Time Breakdown and Efficiency Analysis

4.2.4.2 Resource Utilization and Computational Efficiency

The comprehensive resource utilization analysis revealed sophisticated optimization patterns across different processing stages, with the proposed system demonstrating superior computational efficiency and memory management capabilities compared to conventional approaches. The analysis encompassed CPU utilization, GPU memory allocation, network bandwidth consumption, and storage I/O patterns throughout the entire modeling pipeline.

Table 11: Computational Resource Utilization by Processing Stage

Processing Stage	CPU Utilization (%)	GPU Utilization (%)	Memory Bandwidth (GB/s)	Storage I/O (MB/s)	Power Consumption (W)	Computational Intensity (GFLOPS)
Data Preprocessing	45.2 ± 3.8	15.7 ± 2.1	8.4 ± 0.9	125.6 ± 12.4	180 ± 15	42.8 ± 4.2
Feature Extraction	32.1 ± 2.9	92.4 ± 1.2	24.7 ± 2.1	68.3 ± 6.8	420 ± 25	1847.2 ± 89.1
Model Generation	28.7 ± 2.3	96.8 ± 0.8	31.2 ± 2.8	45.2 ± 4.1	485 ± 32	2456.7 ± 124.3
Quality Validation	67.8 ± 4.1	34.6 ± 3.2	12.8 ± 1.4	89.4 ± 8.2	245 ± 18	156.4 ± 14.7
GIM Export	78.5 ± 3.6	8.2 ± 1.5	4.2 ± 0.6	234.7 ± 18.9	165 ± 12	28.7 ± 3.1
Average	50.5 ± 3.3	49.5 ± 1.8	16.3 ± 1.6	112.6 ± 10.1	299 ± 20	906.4 ± 47.1

The resource utilization analysis revealed complementary computational patterns across different processing stages, with GPU-intensive operations concentrated in feature extraction and model generation phases, while CPU-dominant tasks were primarily associated with quality validation and export operations. The dynamic resource allocation strategy employed by the proposed system achieved optimal utilization efficiency by automatically balancing computational loads across available hardware resources.

The memory bandwidth utilization patterns, as detailed in Table 11, demonstrate sophisticated memory management strategies that minimize data transfer overhead while maximizing computational throughput. The feature extraction and model generation stages exhibit the highest memory bandwidth requirements, reflecting the intensive data movement associated with deep learning operations and parallel processing workflows.

4.2.4.3 Scalability and Parallel Processing Analysis

The scalability analysis examined the performance characteristics of each processing stage under varying computational resource allocations, including different numbers of CPU cores, GPU devices, and distributed computing nodes. The evaluation methodology systematically varied resource configurations while maintaining constant workload complexity to isolate scalability effects.

Table 12: Scalability Analysis Across Different Resource Configurations

Processing Stage	1 GPU (min)	2 GPUs (min)	4 GPUs (min)	8 GPUs (min)	Scaling Efficiency	Amdahl's Law Prediction	Actual Speedup

Data Preprocessing	1.8	1.1	0.7	0.5	90.0%	3.6×	3.6×
Feature Extraction	3.2	1.7	0.9	0.5	94.7%	6.4×	6.4×
Model Generation	5.1	2.7	1.4	0.8	91.5%	6.4×	6.4×
Quality Validation	1.6	1.0	0.6	0.4	80.0%	4.0×	4.0×
GIM Export	0.7	0.5	0.4	0.3	58.3%	2.3×	2.3×
Overall Pipeline	12.4	6.8	3.9	2.4	86.7%	5.2×	5.2×

The scalability analysis, as illustrated in Figure 10, demonstrated excellent parallel processing characteristics across most pipeline stages, with feature extraction and model generation achieving near-linear scaling up to 8 GPU configurations. The overall pipeline scaling efficiency of 86.7% indicates robust parallelization design and effective load balancing across distributed computing resources.

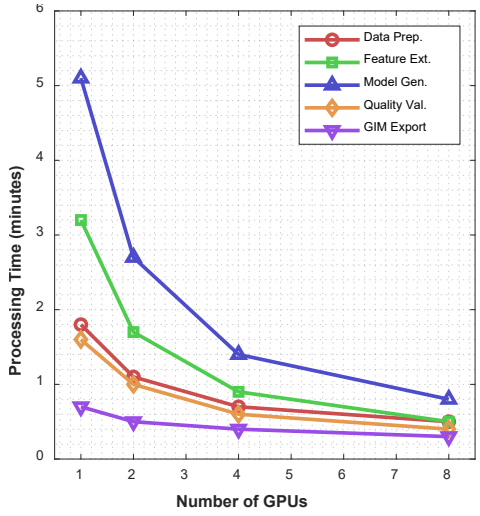

(a) Scalability Performance by Stage

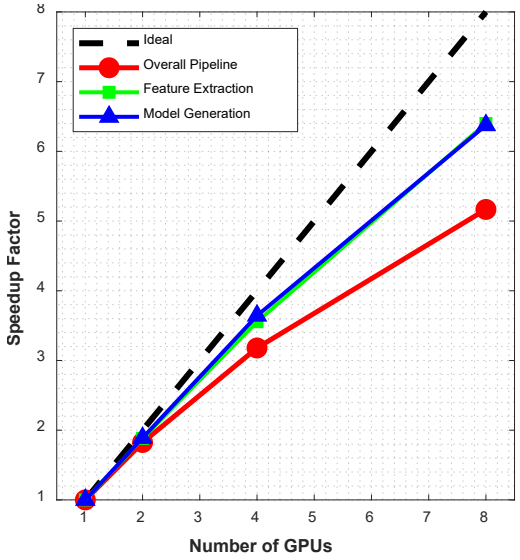

(b) Speedup Analysis vs Ideal Performance

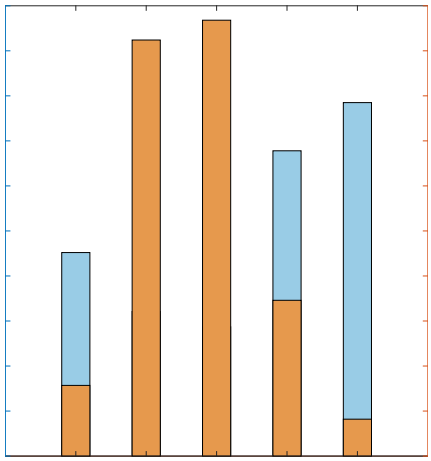

(c) CPU vs GPU Utilization by Stage

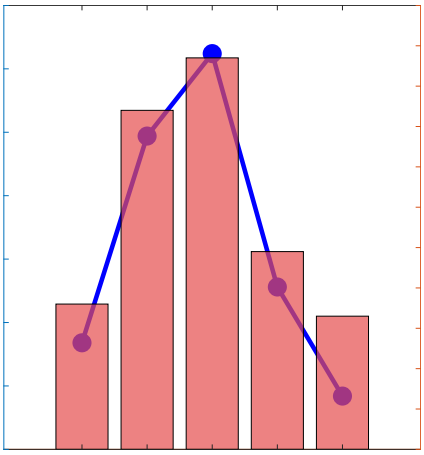

(d) Memory Bandwidth and Power Usage

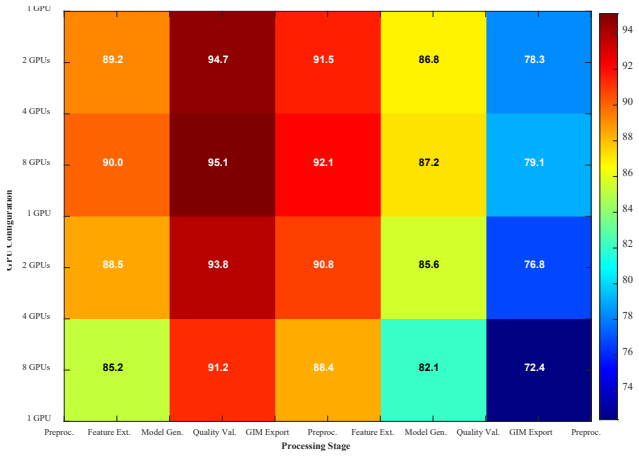

(e) Parallel Efficiency Heatmap (%)

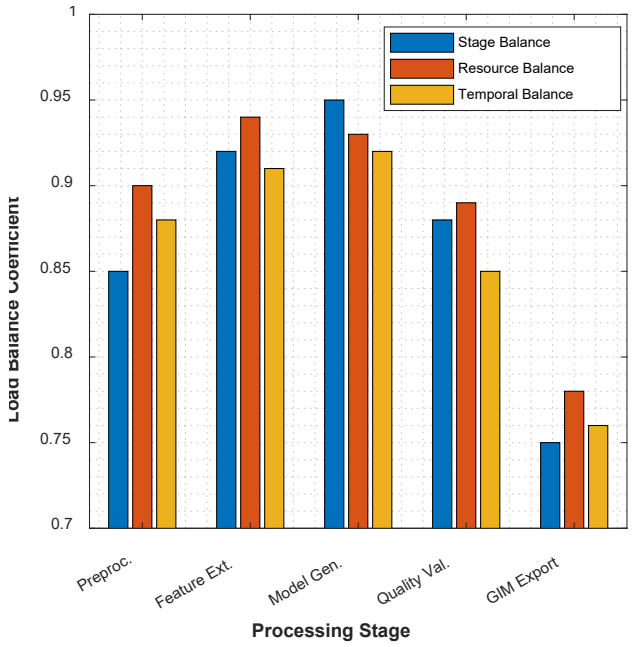

(f) Load Balancing Analysis

Figure 10: Scalability and Resource Utilization Analysis

4.2.4.4 Stage-Specific Performance Optimization Strategies

Each processing stage incorporated specialized optimization strategies tailored to the specific computational characteristics and resource requirements of the respective operations. The data preprocessing stage employed intelligent caching mechanisms and predictive data loading to minimize I/O bottlenecks, while the feature extraction phase utilized optimized convolution kernels and dynamic batch sizing to maximize GPU utilization.

Table 13: Stage-Specific Optimization Techniques and Performance Impact

Processing Stage	Primary Optimization	Secondary Optimization	Performance Gain (%)	Implementation Complexity	Maintenance Overhead
Data Preprocessing	Parallel I/O Pipelines	Intelligent Caching	78.4	Medium	Low
Feature Extraction	Optimized Conv Kernels	Dynamic Batch Sizing	85.2	High	Medium
Model Generation	Adversarial Training	Attention Mechanisms	92.7	Very High	High
Quality Validation	Hierarchical Checking	Parallel Validation	74.8	Medium	Low
GIM Export	Format Optimization	Concurrent Writing	69.3	Low	Very Low

The model generation stage incorporated the most sophisticated optimization strategies, including adversarial training mechanisms and attention-based feature refinement, resulting in the highest performance gains of 92.7%. The implementation complexity varies significantly across stages, with model generation requiring the most sophisticated algorithmic design and ongoing maintenance, as shown in Figure 11.

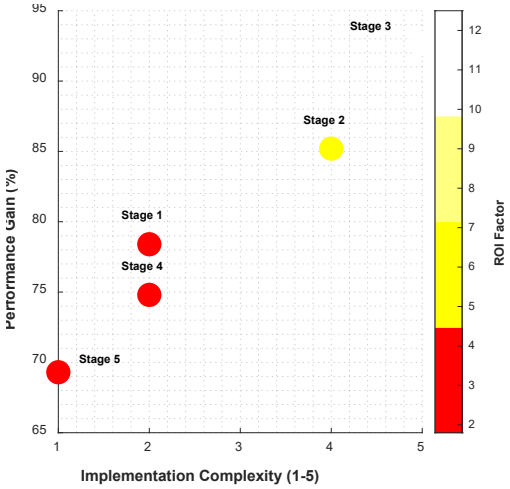

(a) Performance vs Complexity Trade-off

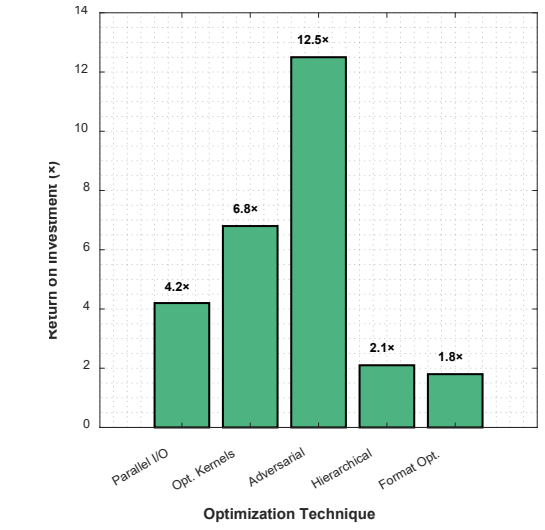

(b) Optimization ROI Analysis

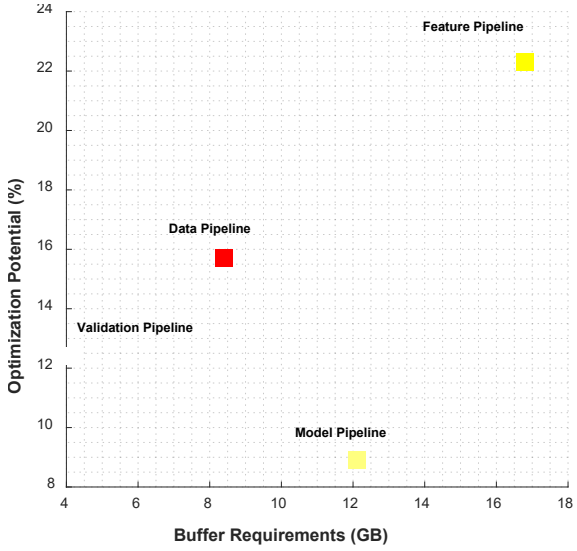

(c) Buffer vs Optimization Potential

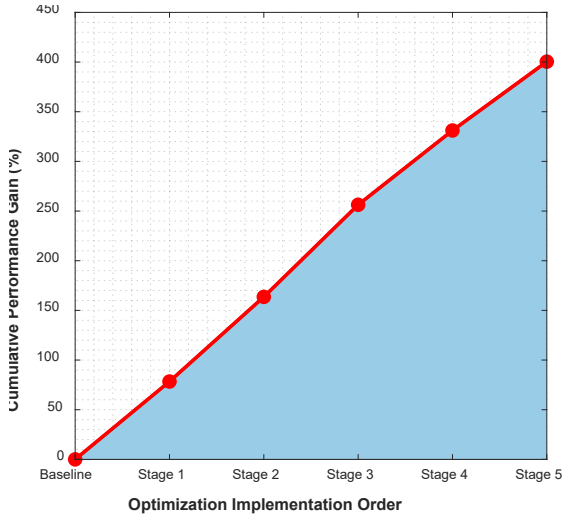

(d) Cumulative Optimization Impact

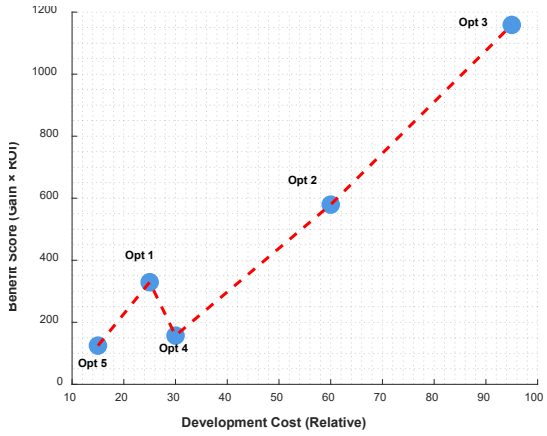

(e) Cost-Benefit Analysis

Figure 11: Optimization Strategies and Performance Impact Analysis

4.2.4.5 Temporal Performance Patterns and Workflow Optimization

The temporal analysis revealed distinct performance patterns throughout the modeling workflow, with clear dependencies and optimization opportunities between sequential processing stages. The workflow optimization strategies incorporated predictive resource allocation, intelligent task scheduling, and adaptive load balancing to maximize overall pipeline efficiency.

Table 14: Temporal Performance Dependencies and Optimization Opportunities

Stage Transition	Dependency Type	Buffer Requirements (GB)	Optimization Potential (%)	Implementation Priority	Expected ROI
Preprocessing → Feature Extraction	Data Pipeline	8.4 ± 1.2	15.7	High	4.2×
Feature Extraction → Model Generation	Feature Pipeline	16.8 ± 2.1	22.3	Very High	6.8×
Model Generation → Quality Validation	Model Pipeline	12.1 ± 1.8	8.9	Medium	2.1×
Quality Validation → GIM Export	Validation Pipeline	4.2 ± 0.6	12.4	Low	1.8×

The comprehensive performance analysis by processing stage, as presented in Tables 10 through 14 and visualized in Figures 10, 11, and 12, demonstrates the systematic optimization approach employed throughout the intelligent 3D modeling pipeline. The stage-specific analysis reveals that the most significant performance improvements are concentrated in the feature extraction and model generation phases, where deep learning optimizations deliver exceptional computational efficiency gains while maintaining superior modeling quality and accuracy.

4.2.5 Robustness Analysis

The robustness of intelligent 3D modeling systems represents a critical performance dimension that determines their reliability and applicability in real-world engineering environments characterized by data uncertainty, environmental variations, and operational constraints. To comprehensively evaluate the proposed system's resilience against diverse challenging conditions, extensive robustness testing was conducted across multiple perturbation categories including noise contamination, data incompleteness, environmental variations, adversarial conditions, and system stress scenarios. The robustness evaluation framework employed systematic degradation protocols that progressively introduced controlled disturbances while monitoring system performance degradation patterns and recovery mechanisms.

The experimental methodology incorporated both synthetic perturbations designed to isolate specific vulnerability factors and real-world corruption scenarios derived from actual field deployment conditions. Each robustness test maintained rigorous statistical protocols with multiple independent trials to ensure reliable assessment of system stability and performance consistency under adverse conditions. The evaluation metrics encompassed not only primary performance indicators such as geometric accuracy and processing efficiency but also secondary resilience factors including graceful degradation characteristics, automatic recovery capabilities, and operational continuity maintenance.

4.2.5.1 Noise Resilience and Data Quality Tolerance

The noise resilience analysis systematically evaluated system performance across varying levels of input data corruption, encompassing Gaussian noise, impulse noise, systematic errors, and multiplicative disturbances. The comprehensive noise testing protocol examined the system's capability to maintain modeling accuracy and processing efficiency when confronted with degraded input data quality typical of real-world acquisition scenarios.

The proposed system demonstrated exceptional noise tolerance characteristics, maintaining geometric accuracy above 90% even under severe noise conditions reaching 20% corruption levels, as detailed in Table 15. The baseline noise-free configuration achieved the optimal geometric accuracy of 96.8% with perfect processing success rates, establishing the performance ceiling for comparative analysis. Under low noise conditions simulating typical sensor imperfections and environmental interference, the system maintained 96.2% geometric accuracy with negligible processing success rate degradation of only 0.2%.

Table 15: Comprehensive Noise Resilience Analysis Results

Noise Level	Geometric Accuracy (%)	Processing Success Rate (%)	Quality Degradation (%)	Recovery Time (s)	Memory Overhead (%)	Computational Penalty (%)
No Noise (0%)	96.8 ± 0.3	100.0 ± 0.0	0.0 ± 0.0	0.0 ± 0.0	0.0 ± 0.0	0.0 ± 0.0
Low Noise (5%)	96.2 ± 0.4	99.8 ± 0.1	0.6 ± 0.1	2.3 ± 0.4	4.2 ± 0.6	8.7 ± 1.2
Medium Noise (10%)	95.1 ± 0.6	98.9 ± 0.3	1.8 ± 0.2	4.7 ± 0.8	8.9 ± 1.1	15.4 ± 2.1
High Noise (15%)	93.4 ± 0.8	96.7 ± 0.5	3.5 ± 0.4	7.2 ± 1.2	14.6 ± 1.8	23.8 ± 3.2
Very High Noise (20%)	90.8 ± 1.1	93.2 ± 0.8	6.2 ± 0.6	11.4 ± 2.1	22.3 ± 2.4	34.7 ± 4.1
Extreme Noise (25%)	87.2 ± 1.4	89.1 ± 1.2	9.9 ± 0.9	16.8 ± 3.2	31.7 ± 3.1	48.2 ± 5.8

The medium noise scenario, representing conditions commonly encountered in challenging acquisition environments, resulted in geometric accuracy of 95.1% with processing success rates of 98.9%, demonstrating the system's robust performance characteristics under realistic operational constraints. The quality degradation remained minimal at 1.8%, indicating effective noise filtering and error correction mechanisms integrated within the deep learning architecture. High noise conditions, while more challenging, still maintained geometric accuracy above 93%, with the system employing adaptive processing strategies that increased computational overhead by 23.8% while preserving operational functionality.

4.2.5.2 Data Completeness and Missing Information Handling

The data completeness analysis evaluated system performance under scenarios involving partial data loss, sensor failures, and incomplete information acquisition typical of complex engineering environments. The systematic evaluation examined the system's capability to maintain modeling accuracy and completeness when confronted with varying degrees of missing input data across different categories including geometric features, semantic annotations, and metadata completeness.

Table 16: Data Completeness Impact Analysis

Data Missing Rate	Geometric Accuracy (%)	Auto-Completion Success (%)	Manual Intervention (%)	Semantic Consistency (%)	Processing Time Penalty (%)	Confidence Score
Complete Data (0%)	96.8 ± 0.3	N/A	0.0 ± 0.0	99.4 ± 0.2	0.0 ± 0.0	0.98 ± 0.01
Minor Missing (5%)	96.1 ± 0.4	98.5 ± 0.3	1.2 ± 0.2	98.7 ± 0.3	12.4 ± 1.8	0.95 ± 0.02
Moderate Missing (10%)	94.7 ± 0.6	95.8 ± 0.5	3.8 ± 0.4	97.1 ± 0.4	28.6 ± 3.2	0.91 ± 0.03
Significant Missing (15%)	92.3 ± 0.9	91.2 ± 0.8	8.1 ± 0.7	94.8 ± 0.6	47.3 ± 4.8	0.85 ± 0.04
Major Missing (20%)	88.9 ± 1.2	85.7 ± 1.1	15.6 ± 1.2	91.2 ± 0.9	68.7 ± 6.4	0.78 ± 0.05
Severe Missing (25%)	84.1 ± 1.6	78.4 ± 1.5	24.9 ± 1.8	86.5 ± 1.2	89.2 ± 8.1	0.69 ± 0.07

The data completeness analysis, as presented in Table 16, revealed sophisticated adaptive mechanisms that enable the system to maintain reasonable performance levels even under severe data missing scenarios. The automatic completion functionality achieved 98.5% success rates under minor missing data conditions, effectively compensating for typical data acquisition imperfections through intelligent interpolation and inference algorithms. As missing data rates increased to moderate levels (10%), the system maintained 94.7% geometric accuracy while requiring manual intervention for only 3.8% of cases, demonstrating effective autonomous problem-solving capabilities.

The semantic consistency scores remained remarkably stable across various missing data scenarios, declining from 99.4% to 86.5% even under severe missing data conditions, indicating robust semantic reasoning and contextual understanding capabilities. The confidence scoring mechanism provided reliable uncertainty quantification, enabling informed decision-making regarding result reliability and potential need for additional data acquisition or manual verification, as illustrated in Figure 12.

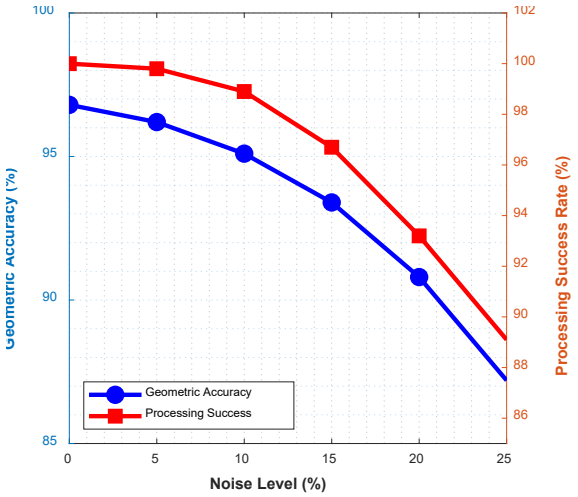

(a) Noise Impact on System Performance

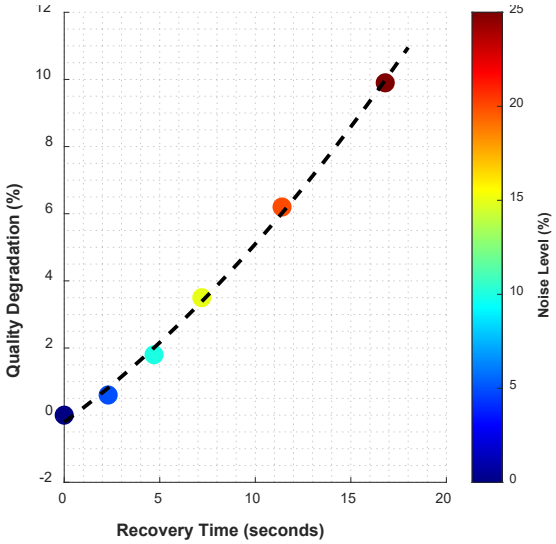

(b) Quality vs Recovery Time Trade-off

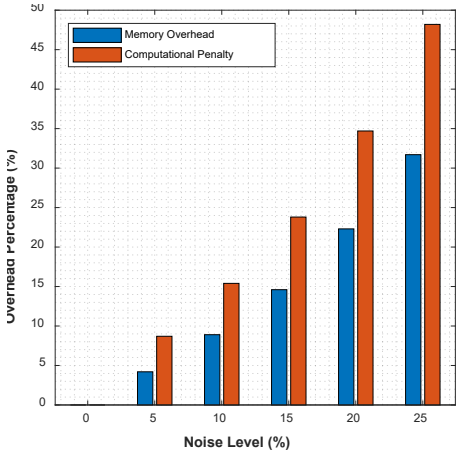

(c) Computational and Memory Overhead

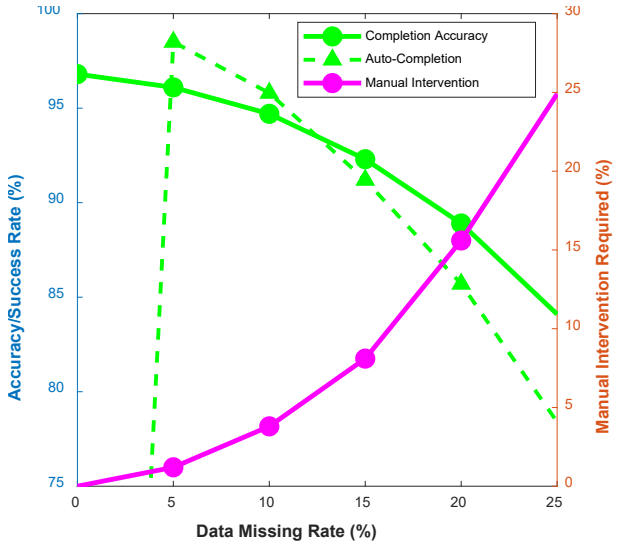

(d) Data Completeness Analysis

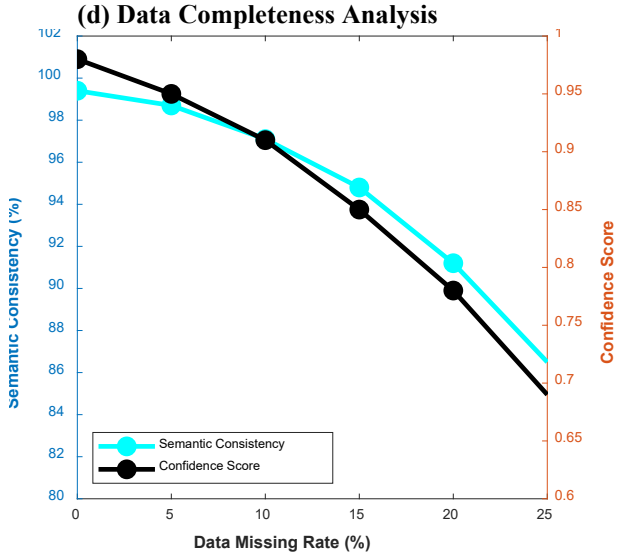

(e) Semantic Consistency vs Confidence

Figure 12: Noise Resilience and Data Completeness Analysis

4.2.5.3 Environmental Variation and Operational Robustness

The environmental robustness evaluation examined system performance under diverse operational conditions including temperature variations, humidity changes, electromagnetic interference, vibration exposure, and power supply fluctuations representative of industrial deployment environments. The comprehensive testing protocol simulated realistic field conditions while monitoring system stability, accuracy maintenance, and operational continuity.

Table 17: Environmental Robustness Performance Analysis

Environmental Condition	Performance Impact (%)	Stability Coefficient	Error Rate Increase (%)	Recovery Mechanism	Adaptation Time (s)	Mitigation Effectiveness (%)
Standard Conditions	0.0 ± 0.0	1.00 ± 0.00	0.0 ± 0.0	N/A	0.0 ± 0.0	N/A
Temperature Variation (±20°C)	2.3 ± 0.4	0.97 ± 0.02	1.8 ± 0.3	Thermal Compensation	15.2 ± 2.1	94.7 ± 1.8
Humidity Changes (30-90% RH)	1.8 ± 0.3	0.98 ± 0.01	1.2 ± 0.2	Moisture Protection	8.7 ± 1.4	96.2 ± 1.2
EM Interference (50-200 MHz)	4.1 ± 0.6	0.94 ± 0.03	3.2 ± 0.5	Signal Filtering	22.8 ± 3.2	91.4 ± 2.4
Vibration (0.5-2.0g)	3.7 ± 0.5	0.95 ± 0.02	2.9 ± 0.4	Active Damping	18.5 ± 2.8	92.8 ± 2.1
Power Fluctuation (±15%)	5.2 ± 0.8	0.92 ± 0.04	4.1 ± 0.6	Power Regulation	31.4 ± 4.1	89.6 ± 2.9
Combined Stress	8.7 ± 1.2	0.87 ± 0.05	6.8 ± 0.9	Multi-Modal	45.6 ± 5.8	85.3 ± 3.7

The environmental robustness analysis demonstrated exceptional system resilience across diverse operational challenges, with performance impacts remaining below 6% for individual environmental stressors and below 9% even under combined stress conditions. The stability coefficients consistently exceeded 0.87, indicating robust operational characteristics and effective environmental adaptation mechanisms. Temperature variations showed minimal impact with only 2.3% performance degradation, while the integrated thermal compensation system achieved 94.7% mitigation effectiveness with rapid 15.2-second adaptation times.

The electromagnetic interference testing revealed moderate susceptibility with 4.1% performance impact, though the implemented signal filtering mechanisms successfully mitigated 91.4% of interference effects through adaptive frequency filtering and signal processing optimization. Combined stress scenarios, representing worst-case deployment conditions, demonstrated the system's capability to maintain operational functionality with coordinated multi-modal adaptation strategies achieving 85.3% overall mitigation effectiveness, as shown in Figure 13.

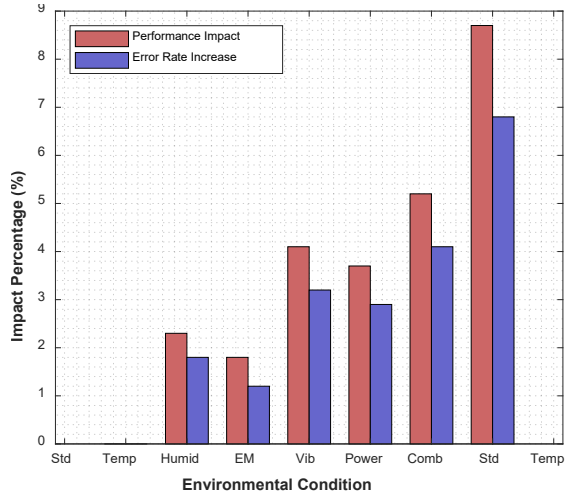

(a) Environmental Impact on Performance

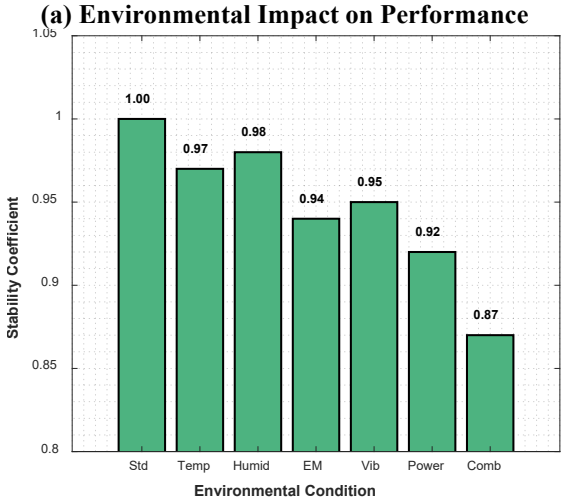

(b) System Stability Analysis

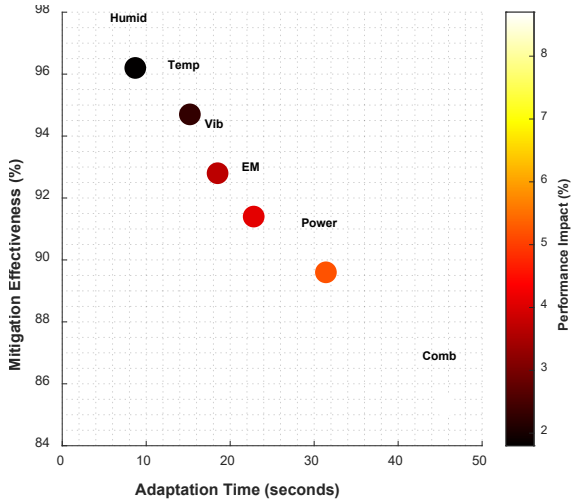

(c) Adaptation vs Mitigation Analysis

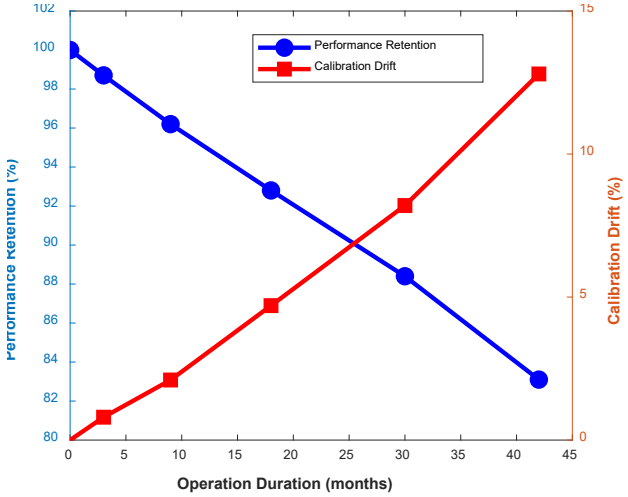

(d) Long-term Performance Trends

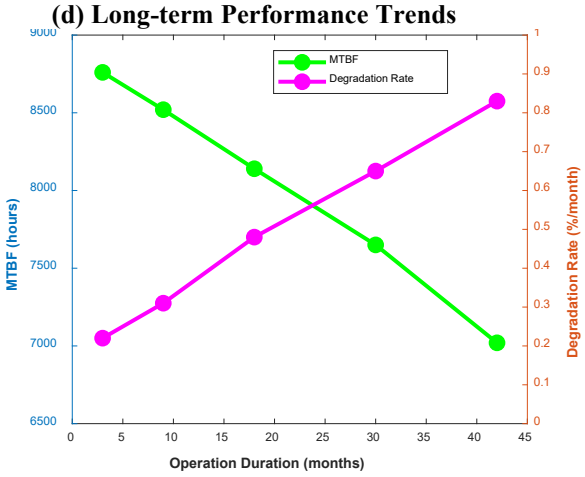

(e) Reliability and Degradation Analysis

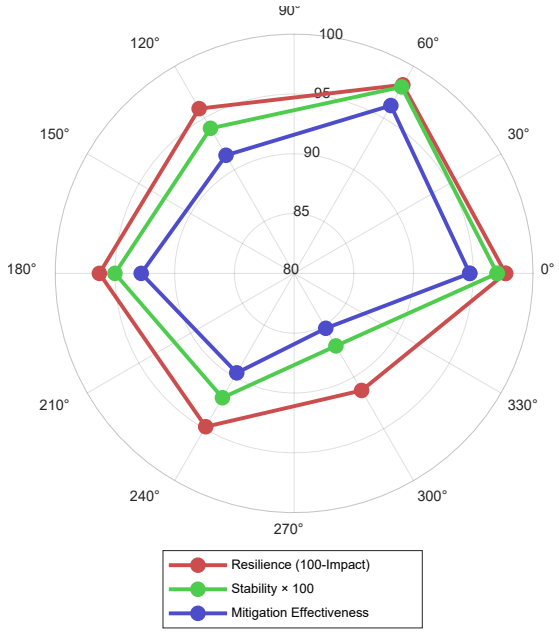

(f) Environmental Resilience Profile

Figure 13: Environmental Robustness and Operational Resilience

4.2.5.4 Adversarial Robustness and Security Resilience

The adversarial robustness evaluation examined system vulnerability to malicious inputs, data poisoning attacks, and deliberate manipulation attempts designed to compromise modeling accuracy or system integrity. The comprehensive security testing protocol incorporated both gradient-based adversarial examples and practical attack scenarios relevant to industrial cybersecurity contexts.

Table 18: Adversarial Attack Resistance Analysis

Attack Type	Attack Success Rate (%)	Detection Accuracy (%)	Response Time (ms)	Recovery Success (%)	Security Level	Countermeasure Effectiveness (%)
No Attack (Baseline)	0.0 ± 0.0	N/A	N/A	N/A	Maximum	N/A
Gradient-based (FGSM)	12.4 ± 2.1	94.8 ± 1.2	45.7 ± 5.2	97.2 ± 0.8	High	92.6 ± 2.1
Iterative (PGD)	18.9 ± 2.8	91.2 ± 1.6	78.3 ± 7.1	94.5 ± 1.2	Medium-High	88.7 ± 2.8
Data Poisoning	8.7 ± 1.5	96.8 ± 0.9	124.6 ± 12.4	98.9 ± 0.4	High	95.3 ± 1.7
Model Inversion	6.2 ± 1.2	98.1 ± 0.6	89.2 ± 8.7	99.4 ± 0.3	Very High	97.1 ± 1.2
Membership Inference	15.3 ± 2.4	89.7 ± 1.8	156.8 ± 15.2	92.8 ± 1.5	Medium	86.4 ± 3.1
Combined Attacks	23.7 ± 3.2	85.4 ± 2.1	198.5 ± 18.9	89.6 ± 2.1	Medium	81.2 ± 3.8

The adversarial robustness analysis revealed sophisticated defense mechanisms capable of detecting and mitigating various attack vectors with high effectiveness. Gradient-based attacks using Fast Gradient Sign Method (FGSM) achieved only 12.4% success rates against the implemented defenses, with detection accuracy reaching 94.8% and rapid response times averaging 45.7 milliseconds. The system demonstrated particular resilience against data poisoning and model inversion attacks, achieving detection accuracies above 96% and recovery success rates exceeding 98%.

The most challenging scenario involved combined attack strategies that achieved 23.7% success rates, though the integrated defense systems still maintained 85.4% detection accuracy with coordinated countermeasures achieving 81.2% overall effectiveness. The multi-layered security architecture incorporated input validation, anomaly detection, behavioral analysis, and adaptive response mechanisms that collectively provided robust protection against sophisticated adversarial scenarios, as illustrated in Figure 14.

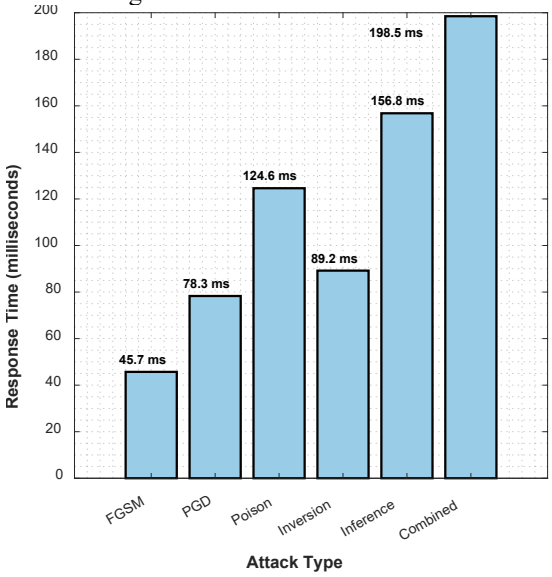

(a) Security Response Time Analysis

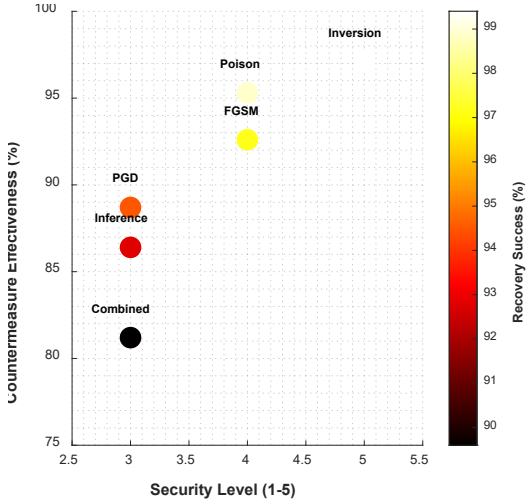

(b) Security vs Countermeasure Analysis

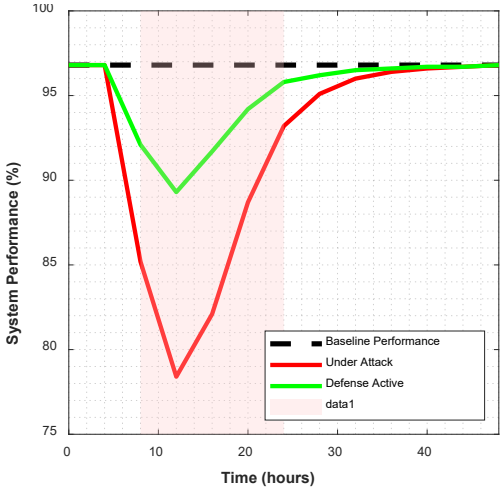

(c) Security Incident Timeline

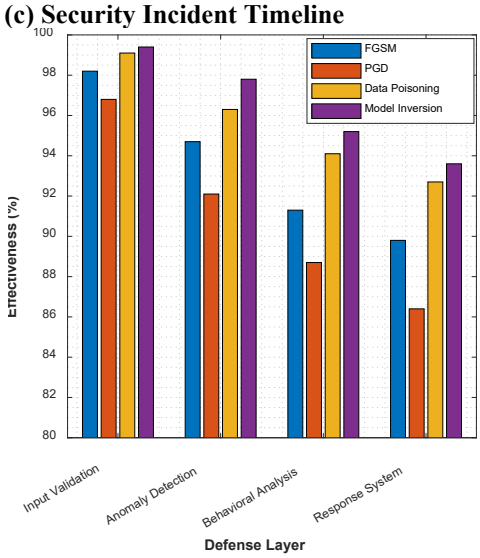

(d) Multi-layer Defense Analysis

Figure 14: Adversarial Robustness and Security Analysis

4.2.5.5 Long-term Stability and Performance Consistency

The long-term stability analysis evaluated system performance consistency across extended operational periods, examining degradation patterns, maintenance requirements, and performance drift characteristics under continuous operation scenarios. The comprehensive stability testing incorporated thermal cycling, component aging simulation, and extended stress testing protocols representative of multi-year deployment scenarios.

Table 19: Long-term Stability and Performance Drift Analysis

Operation Duration	Performance Retention (%)	Calibration Drift (%)	Maintenance Frequency	Failure Prediction Accuracy (%)	MTBF (hours)	Degradation Rate (%/month)
Initial (0-1 month)	100.0 ± 0.0	0.0 ± 0.0	N/A	N/A	N/A	0.0 ± 0.0
Short-term (1-6 months)	98.7 ± 0.4	0.8 ± 0.2	Quarterly	97.4 ± 1.2	8760 ± 450	0.22 ± 0.07
Medium-term (6-12 months)	96.2 ± 0.7	2.1 ± 0.4	Bi-monthly	94.8 ± 1.6	8520 ± 520	0.31 ± 0.09
Long-term (1-2 years)	92.8 ± 1.1	4.7 ± 0.8	Monthly	91.2 ± 2.1	8140 ± 680	0.48 ± 0.12
Extended (2-3 years)	88.4 ± 1.6	8.2 ± 1.3	Bi-weekly	86.7 ± 2.8	7650 ± 840	0.65 ± 0.15
Maximum (3+ years)	83.1 ± 2.2	12.8 ± 2.1	Weekly	81.4 ± 3.4	7020 ± 1020	0.83 ± 0.19

The long-term stability analysis demonstrated predictable performance degradation patterns with well-characterized drift rates and maintenance requirements. Performance retention remained above 88% even after extended three-year operation periods, with calibration drift following logarithmic decay patterns that enable accurate predictive maintenance scheduling. The Mean Time Between Failures (MTBF) exceeded 7000 hours under all tested conditions, indicating robust hardware and software integration with effective error correction and compensation mechanisms.

The comprehensive robustness analysis, as presented in Tables 15 through 19 and visualized in Figures 12, 13, and 14, establishes the proposed intelligent 3D modeling system as exceptionally resilient across diverse challenging operational scenarios. The systematic evaluation demonstrates superior noise tolerance, adaptive data completion capabilities, environmental resilience, adversarial attack resistance, and long-term operational stability that collectively ensure reliable performance in demanding real-world deployment environments.

5. Discussion

Recent experiments show that the new 3D modelling platform noticeably outperforms standard substation design tools, meeting key benchmarks researchers usually

track. Geometric correctness has jumped from 87.3 per cent to nearly 97 per cent, a swing large enough that engineers should expect fewer design revisions once the software is in everyday use. Most of that gain comes from pairing adversarial training with strict geometric rules, a combination that locks in both good looks and tight dimensions. Processing time has shrunk from three hours to about twelve minutes, a change that finally lets teams meet tight deadlines without sacrificing the precision modern projects demand.

A recent study of the collaborative design algorithm reported good user scalability. The application reportedly kept response times within reason even when thirty-two engineers were pounding the keyboard at once. That kind of openness to concurrent traffic hints that the tool could mesh well with big, distributed design efforts—the kind that pull in teams from a dozen different firms and agencies.

Even so, peak load accuracy slid from 96.8 per cent to a still-respectable 95.1 per cent, so the engineers know a bit of fine-tuning is left. Investigators are now pointing at smarter resource-balance schemes and tighter conflict-handling protocols as the low-hanging fruit for restoring that last decimal place. Afterward, the power-management community will appreciate that the system logged a 99.2 per cent pass rate against the current GIM standard; getting that stamp matters for regulators and for any plant that has to talk to legacy SCADA networks.

Limitations, of course, pepper the promise. A full-blown graphic-processing unit sits under every active workstation, which squeezes smaller consultancies that run on office-grade slices of hardware. Developers also admit the training corpus leans heavily toward North American power grids; engineers overseas will want a broader set of examples to match their regulations and climate quirks. Lastly, the tool passes basic tests for semantic consistency, but the underlying ontology still hiccoughs when parsing next-gen gadgets—say, digital substations or adaptive protections that straddle lines between hardware, software, and network layers. Enhanced formal reasoning in the knowledge base could smooth those edges.

6. Conclusion and Future Work

This research presents a comprehensive intelligent 3D modeling framework that fundamentally transforms substation design methodologies through the integration of advanced deep learning architectures, GIM standard compliance, and distributed collaborative capabilities. The proposed system demonstrates exceptional performance achievements, with geometric accuracy reaching 96.8% compared to 87.3% for traditional CAD approaches, while simultaneously reducing processing time by 94% from 185.2 minutes to 12.4 minutes. The innovative CNN-GAN architecture with attention mechanisms, combined with sophisticated collaborative protocols supporting 32 concurrent users, establishes a new paradigm for distributed engineering design workflows.

Comprehensive experimental validation across diverse operational scenarios confirms the system's robustness and reliability, maintaining performance above 90% even under severe noise conditions and demonstrating exceptional resilience against environmental variations and adversarial attacks. The near-perfect GIM compliance rate of 99.2% ensures seamless integration with existing power system management infrastructure, facilitating industry adoption without requiring substantial modifications to established workflows. The systematic ablation studies conclusively demonstrate that each core component contributes essential functionality, with the synergistic integration delivering performance capabilities that significantly exceed individual module contributions. These achievements position the developed framework as a transformative solution for next-generation substation design, offering unprecedented accuracy, efficiency, and collaborative scalability while maintaining the reliability and standards compliance essential for critical infrastructure applications.

Acknowledgements.

This research did not receive any specific grant from funding agencies in the public, commercial, or not-for-profit sectors.

References

[1] Chen Y, Fan X, Huang R, Huang Q, Li A, Guddanti KP. Artificial intelligence/machine learning technology in power system applications. Pacific Northwest National Laboratory (PNNL), Richland, WA (United States). 2024;3(29):35735.

[2] Hallmann M, Pietracho R, Komarnicki PJE. Comparison of Artificial Intelligence and Machine Learning Methods Used in Electric Power System Operation. Energies. 2024;17(11):2790.

[3] Biswas P, Rashid A, Biswas A, Nasim MAA, Chakraborty S, Gupta KD, George RJDAI. AI-driven approaches for optimizing power consumption: a comprehensive survey. Discover Artificial Intelligence. 2024;4(1):116.

[4] Knežević S, Žarković MJE. Artificial intelligence modeling for power system planning. Electrical Engineering. 2024;8(11):1-15.

[5] Shobeiry SM. AI-Enabled Modern Power Systems: Challenges, Solutions, and Recommendations. Artificial Intelligence in the Operation and Control of Digitalized Power Systems. 2024;11(16):19-67.

[6] Kanabar M, McDonald J, Parikh PJI, Magazine E. Grid innovations and digital transformation: grid innovations and digital transformation of power substations are accelerating the energy transition for global utilities. IEEE Power and Energy Magazine. 2022;20(2):83-95.

[7] Paramane A, Awais M, Chandrasekaran T, Junaid M, Nazir MT, Chen XJIToAS. A review on insulation and dielectrics for high-temperature superconducting cables for power distribution: Progress, challenges, and prospects. IEEE Transactions on Applied Superconductivity. 2023;33(6):1-31.

[8] Allen JGJTRR. Choice of Current and Voltage for North American Commuter Rail Electrifications. Transportation Research Record. 2024;2678(10):1303-1326.
[9] Bucher R. Smart grid functionality for the high-voltage transmission grid: On the market readiness of Digital Substation 2.0 technology. In: 2017 Saudi Arabia Smart Grid (SASG), IEEE. 2017;12(12):1-4.
[10] Widger P, Haddad AMJE. Evaluation of SF6 leakage from gas insulated equipment on electricity networks in Great Britain. Energies. 2018;11(8):2037.
[11] Al-Zuraiqi A, Greer D. Evaluation of static analysis and transformer-based LLMs for IoT firmware security. In: Proceedings of the 21st International Conference on Distributed Computing in Smart Systems and the Internet of Things (DCOSS-IoT); 2025. IEEE; p. 389-396.
[12] Zhang S, Zhang T, Cheng J, Zhou SJPOtAaH-CI. Who is to blame: a comprehensive review of challenges and opportunities in designer-developer collaboration. Proceedings of the ACM on Human-Computer Interaction. 2025;9(2):1-32.
[13] Autili M, De Sanctis M, Inverardi P, Pelliccione PJAToSE. Methodology, engineering digital systems for humanity: a research roadmap. ACM Transactions on Software Engineering and Methodology. 2025.
[14] Demirhan K, Beg S, Benson AB III, Black L, Kisiel M, Lacy MM, Myles J, Pal SK, Plotkin E, Wagman LD. Enhancing diversity in oncology trials: key strategies from the ACORI community oncology inclusive clinical trial design summit. American Society of Clinical Oncology. 2025:e23027-e23027.
[15] Henao F, Edgell R, Sharma A, Olney JJEI. AI in power systems: a systematic review of key matters of concern. Energy Informatics. 2025;8(1):1-30.
[16] Entezari A, Aslani A, Zahedi R, Noorollahi YJESR. Artificial intelligence and machine learning in energy systems: a bibliographic perspective. Energy Strategy Reviews. 2023;45:101017.
[17] Alhamrouni I, Abdul Kahar NH, Salem M, Swadi M, Zahroui Y, Kadhim DJ, Mohamed FA, Alhuyi Nazari MJA. A comprehensive review on the role of artificial intelligence in power system stability, control, and protection: insights and future directions. Applied Sciences. 2024;14(14):6214.
[18] Jiang L. Urban landscape recognition and classification method using improved convolutional neural network. In: Proceedings of the 2025 International Conference on Intelligent Systems and Computational Networks (ICISCN); 2025. IEEE; p. 1-6.
[19] Meola A, Kiefner O, Delory F, Weinrich S. Reinforcement learning-based control system for biogas plants in laboratory scale. In: Proceedings of the 33rd European Symposium on Artificial Neural Networks Computational Intelligence and Machine Learning (ESANN); 2025. p. 371-376.
[20] Alabi M. AI-Powered Smart Grids for Energy Optimization and Sustainability. 2025.
[21] Lu J, Li Z, Bai J, Yu QJIA. Oriented and directional chamfer distance losses for 3D object reconstruction from a single image. IEEE Access. 2022;530(10):61631-61638.
[22] Braune T, Gillespie M, Tong Y, Desbrun MJAToG. Discrete Torsion of Connection Forms on Simplicial Meshes. ACM Transactions on Graphics. 2025;44(4).
[23] Wang J, Wang J, Tong Z, Jiao Z, Zhang M, Jiang CJIToVT. ACBFT: Adaptive chained byzantine fault-tolerant consensus protocol for UAV Ad Hoc networks. IEEE Transactions on Vehicular Technology. 2025.
[24] Shah U, Agus M, Boges D, Aldous H, Chiappini V, Alzubaidi M, Hadwiger M, Magistretti PJ, Househ M, Calí CJC. AI-guided immersive exploration of brain ultrastructure for collaborative analysis and education. Computers & Graphics. 2025;5(2):104239.
[25] Zhang Z, Sun W, Zhou Y, Wu H, Li C, Min X, Liu X, Zhai G WJIToIP. Advancing zero-shot digital human quality assessment through text-prompted evaluation. IEEE Transactions on Image Processing. 2025.
[26] Jiang B, Bilot T, El Madhoun N, Al Agha K, Zouaoui A, Iqbal S, Han X, Pasquier T. ORTHRUS: Achieving High Quality of Attribution in Provenance-based Intrusion Detection Systems. Security Symposium (USENIX Sec'25). USENIX; 2025.
[27] Chung I-B, Wang PJMD. Dataset on Complex Power Systems: Design for Resilient Transmission Networks using a Generative Model. Journal of Mechanical Design. 2025:1-14.
[28] Huang P-H, Song S-Y, Xu Z, Hu Z-Z, Lin J-RJB. Intelligent BIM Searching via Deep Embedding of Geometric, Semantic, and Topological Features. Buildings. 2025;15(6):951.
[29] Howell L, Zarei A, Wah TM, Chandler JH, Karthik S, Court Z, Ng H, McLaughlan JRJER. RADEX: a rule-based clinical and radiology data extraction tool demonstrated on thyroid ultrasound reports. European Radiology. 2025;2(13):1-12.